

THE SOUTH ECLIPTIC POLE REGION:
STELLAR POPULATIONS AND PROPER
MOTIONS



FREIE WISSENSCHAFTLICHE ARBEIT ZUR
ERLANGUNG DES GRADES
DIPLOM-PHYSIK

eingereicht am 31.03.2017
Institut für Physik und Astronomie
der
Mathematisch-Naturwissenschaftlichen Fakultät
der
Universität Potsdam
von

Thomas Schmidt

1. Gutachter: Prof. Dr. Maria-Rosa Cioni
 2. Gutachter: Dr. Ralf Scholz
- Potsdam, den 31. März 2017

Zusammenfassung

Um die Eigenbewegungen von Sternpopulation in Feldern zu untersuchen, die vom VISTA Survey des Systems der Magellanschen Wolken (VMC) beobachtet wurden, wurde ein Python Skript entwickelt. Dieses Skript nutzte mehreporchige Beobachtungen im Infrarotbereich, die 26896 Galaxies und 154699 Sterne umfassten mit einer K Magnitude < 19 , um die Mediane der Eigenbewegungen von Populationen verschiedenen Alters zu berechnen. Die Messungen umfassen eine Zeitspanne von einem Jahr und die Populationen wurden anhand ihrer Verteilung im Farben-Helligkeits-Diagramm mit K und J-K Magnituden unterschieden. Die zur Berechnung der Eigenbewegungen genutzte Methode wurde in Cioni et al.(2016) veröffentlicht. Die Eigenbewegung wurde mit der Methode der kleinsten Quadrate einer linearen Ausgleichsgeraden berechnet und die Galaxien wurden genutzt um einen absoluten astrometrischen Referenzrahmen zu erstellen. Die Ergebnisse waren konsistent mit früheren Arbeiten und wiesen kleinere Fehlerbalken vor. Für das Feld im äußeren Bereich der Großen Magellanschen Wolke das LMC 8.8 genannt wird, wurde der Median der Eigenbewegung bestimmt als $\mu_\alpha \cos \delta = 2,20 \pm 0.16 \text{mas/a}$ und $\mu_\delta = 1.68 \pm 0.17 \text{mas/a}$. Milchstraßensterne im Vordergrund des Feldes konnten mit einer Eigenbewegung von $\mu_\alpha \cos \delta = 2.73 \pm 0.17 \text{mas/a}$ und $\mu_\delta = 7.95 \pm 0.17 \text{mas/a}$ ermittelt werden. Außerdem zeigten Berechnungen der Felder STR 1.1 und STR 2.1 im der Magellanschen Wolken, dass annehmbare Mediane der Eigenbewegung in weniger bevölkerten Feldern ermittelt werden können und Streuung der Mediane der Eigenbewegung, gefunden werden kann, was weitere Untersuchungen interessant macht. Außerdem bewies sich das Skript als belastbar gegenüber ungewollten Verschiebungen in den Daten und blieb trotzdem zuverlässig.

Abstract

To study the proper motion proper of stellar populations in fields observed in VISTA survey of the Magellanic Cloud System (VMC) a Python script was developed. This script used multiple epochs of near-infrared observations containing up to 26896 galaxies and 154699 stars with a K magnitude < 19 , to derive the median proper motions for populations of stars of different ages. The baseline of the observations was one year, and the populations were chosen by their distribution in the colour-magnitude diagram in K and J-K magnitudes. The method used to calculate proper motions was published in Cioni et al. (2016). The proper motion was derived by using a linear least square fit and galaxies were used to create an absolute astrometric reference frame. The results were found to be consistent with the previous investigations and could improve on smaller errors bars. For the field of the outer region of Large Magellanic Cloud (LMC), named by LMC 8.8, was a median proper motion of $\mu_\alpha \cos \delta = 2,20 \pm 0.17 \text{mas/yr}$ and $\mu_\delta = 1.68 \pm 0.17 \text{mas/yr}$ was obtained. Milky way stars in this field were found to have a median proper motion of $\mu_\alpha \cos \delta = 2.73 \pm 0.14 \text{mas/yr}$ and $\mu_\delta = 7.95 \pm 0.14 \text{mas/yr}$. Also calculations of the stream fields STR 1.1 and STR 2.1 showed that decent median proper motions could be derived in low populated fields and showed spread in median proper motions for different populations worth of further investigations. Also, the script proved to be resilient to bigger unintended shifts in the data, while still being reliable.

Contents

0.1	introduction	6
0.2	sample selection	9
0.3	data processing	14
0.3.1	astrometric reference frame	14
0.3.2	using the closest galaxy as reference	18
0.4	proper motion calculation	19
0.4.1	proper motion galaxies	20
0.4.2	proper motion conversion	22
0.4.3	The median absolute deviation	23
0.4.4	proper motion stars	26
0.4.5	proper motion LMC stars	31
0.4.6	errors	32
0.5	proper motion results	33
0.6	proper motion centre of mass	34
0.7	VMC stream fields	38
0.7.1	STR 1_1	38
0.7.2	STR 1_1	42
0.8	conclusion	45
0.9	future	46
0.10	acknowledgment	47
0.10.1	Eidesstattliche Erklärung	48

0.1 introduction

The Magellanic clouds offer a great opportunity for us to develop a greater understanding of the local universe. They are some of the closest larger structures outside the milky way. The Large Magellanic Cloud(LMC) is a dwarf galaxy around 50 kiloparsecs[1] away. Their properties are of great concern for many fields in modern astronomy, for example, stellar evolution since they host, zones of recent massive star formation like 30 Doradus[2] , many younger (1-3 Gyr) globular clusters and planetary nebulae. Even, a variety of pulsating stars like RR Lyra and Cepheids[3] were found. Also, many steps in the cosmic distance ladder are heavily based on knowledge about the clouds. In 1912 more than a hundred years ago Henrietta Leavitt used Cepheids solely from the Small Magellanic Cloud (SMC) to derive the periodluminosity relationship, which then enabled Erwin Hubble to determine Hubble law. By calculating the distance to Andromeda(M31) and therefore establishing the idea of an expanding universe. Even the closest supernova in the last in recent history was hosted by the Magellanic clouds (SN 1987A). Since both clouds seem to be gravitationally bound, they can also be used as an example for two minor galaxies merging, where one exceeds the other by mass by far. Thanks to technological improvements many uncertainties in their properties were reduced significantly in the last years. But there are still many things remaining unknown. There are significant uncertainties about their origin and where their actual centres of mass are. Proper motion on a large scale could be a key to many of these problems. However, proper motion measurements and their calculation are highly challenging. The further away, the more difficult it gets. To measure accurate proper motions at the distance of the Magellanic Clouds, very precise measurements have to be done. Key points in measuring proper motions are the angular resolution of the telescope, the signal to noise ratio of the measurements, the number of measurements, reference frame and the baseline of the observations. The VISTA survey of the Magellanic Clouds system lead by Prof. Dr Maria-Rosa Cioni (VMC; Cioni et al. 2011,) aims for accurate proper motion measurements to obtain ways to find a three-dimensional and spatially resolved star formation history of the Magellanic clouds. It was shown[4], that deep ($K < 19$) multi-epoch images taken in K filter and with a long baseline of around 1 year can reproduce results of previous investigations and split population correlated to the clouds from foreground Milkyway stars. The advantage of this survey is this large field view Vista has. Even when taking longer exposure time to gain deeper images, surveying a larger field of the sky like the Magellanic Clouds will be done in a reasonable time. The first method was later refined in Cioni et al. 2016, which significantly reduced the

errors on the median proper motion for different populations. With more accurate measurements these uncertainties could be reduced even further. The Gaia space mission, for example, will provide highly accurate distances and proper motion for some brighter stars in the LMC, which could be used to improve proper motion for a larger sample of stars from VMC. The main challenge for this method is getting a reliable reference frame. The reference frame obtained by the field of galaxies used to reference the positions is highly dependent on how the centres of the galaxies are determined. The quality of the reference frame can be determined by calculating the proper motion of the galaxies used to create the reference frame. This is where this thesis came in place. Its goal was to develop a Python code which can calculate proper motion from VMC catalogues with a variety of populations in LMC and SMC. The field LMC 8.8 was the first field to get proper motions derived with this code. It is located in the outer disk of the LMC and provides an excellent opportunity to compare the results to previous investigations. The two stream fields STR 1.1 and STR 2.1 were used to test the code further and also is the code already in use helping to investigate an improved method for the determination of more accurate galaxies positions. The next figure shows a coverage map¹ of the VMC survey, where fields used in this thesis are marked to see their position on the southern hemisphere.

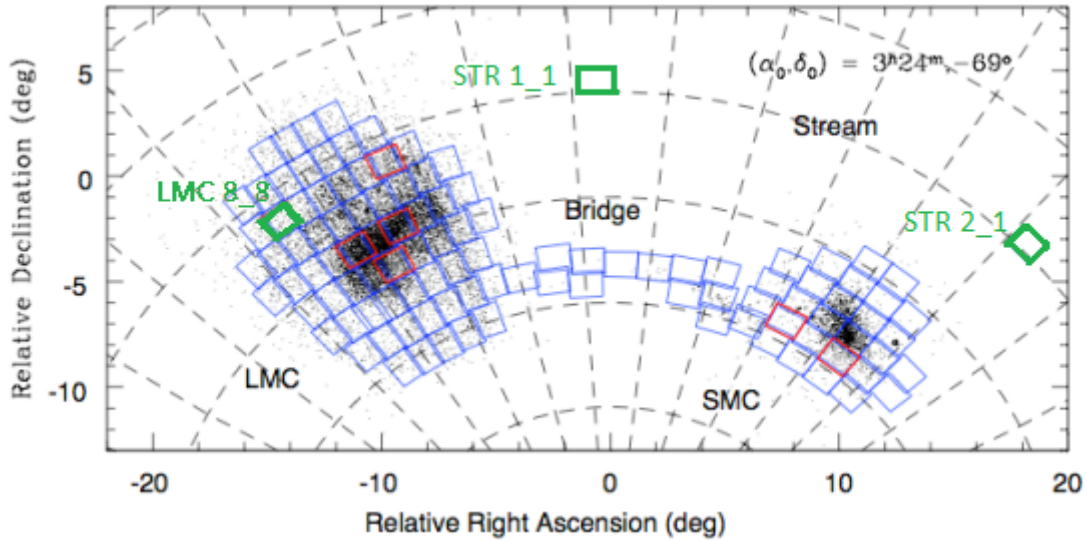


Figure 1: VMC coverage map green marked fields were used in this thesis. The figure was taken from VMC ESO Phase 3 Data Release Description

The data catalogues used for this thesis are provided by the VISTA Sci-

¹<https://www.eso.org/sci/observing/phase3/news.html>

ence Archive (VSA²) and generated by the VISTA IR Camera (VIRCAM) on the Visible and Infrared Survey Telescope for Astronomy (VISTA) operated by the European Southern Observatory (ESO) and located at ESO's Paranal Observatory in northern Chile. The VIRCAM is a near-infrared imaging camera, and it consists of 16 VIRGO HgCdTe near-infrared detectors[5] each with a resolution of 2048 by 2048 pixel. Resulting in a 0.6 square deg active field of view, spanning over a large field of view and a resolution of 67Mpixels. In mean every pixel represents 0.339 arcsec. Measurements in Z, Y, J, H, K_s and two narrowband filters are available. VISTA is currently the fastest survey telescope in the near-infrared, due to its large field of view.

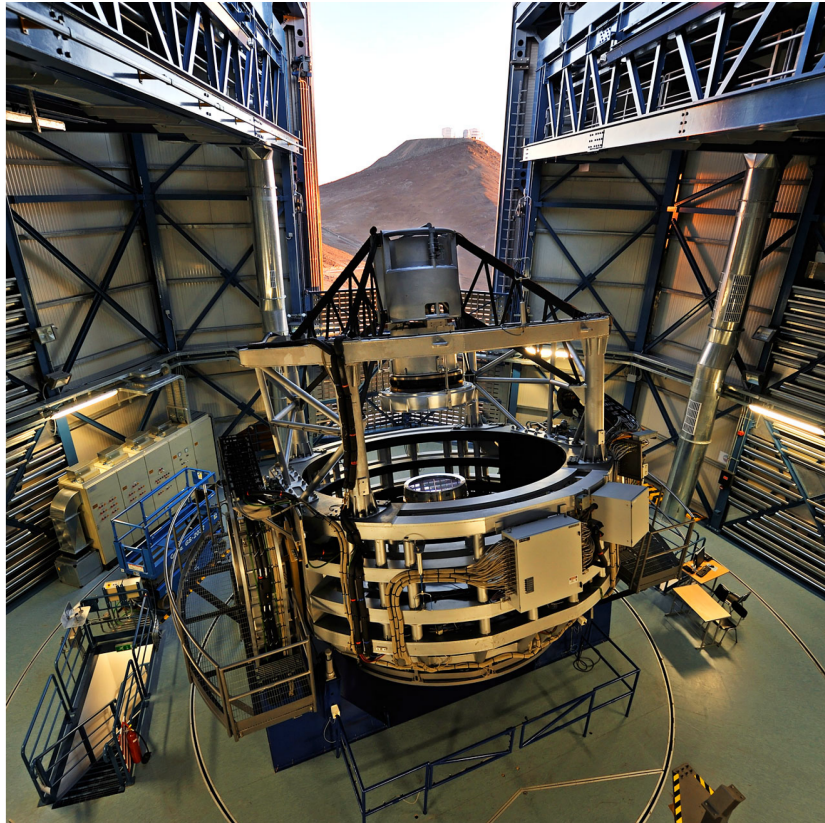


Figure 2: VISTA telescope with VLTs in the background (Photo credit: G.Hudepohl / ESO taken from Sutherland et al. 2015)

For this thesis, only data obtained with the K filter was used. The raw images were ingested by the standard data pipeline at the Cambridge Astronomical Survey Unit (CASU³). At CASU corrections were done by using

²<http://horus.roe.ac.uk/vsa/index.html>

³<http://www.ast.cam.ac.uk/mike/casu/>

dark frames, flat-fields and stacking the jitter images. Also, sources were classified, and precise positions on the CCD were calculated. Later are essential to the proper motion calculation. Due to seeing this can be difficult, resulting in larger uncertainties. Especially the positions of galaxies that are later used to create a reference frame, since they are already not optimal point sources and them getting blurred increases the problem. That is the reason for using K filter images only. In K filter the central positions can be better located with fewer uncertainties. K filter images of galaxies since the picture the mass distribution of galaxies way better. Space telescopes like the Hubble Space Telescope and Gaia are way more precise in angular resolutions than ground-based telescopes like VISTA since the are not affected by seeing. However, longer baselines and larger fields of view are essential to extensive surveys and benefit ground-based astronomy. Technologies like adaptive optics are going to increase precision and especially large infra-red telescopes will benefit trough that, since currently adaptive optics on large telescopes is only possible in infra-red. However, new methods like advanced machine learning⁴ will revolutionise astronomy computations. In recent years, data samples sizes in modern astronomy got way bigger going from large tables to even bigger data cubes.

0.2 sample selection

The data catalogues used in this thesis were provided by the VISTA Science Archive (VSA), and they are available since VMC data release 3. They were directly queried by using an SQL query resulting six catalogues for objects classified as galaxies, one for each pointing and 12 catalogues for objects classified as stars. The 12-star-catalogues had two files per pointing since the number of source per query was limited by five hundred thousand by the VSA. The first column (Upload ID) of the catalogues plays a significant role in processing the data since every Upload ID corresponds directly to a single unique detected sources. The fact that the VSA query had split the star catalogues due to their size resulted in the problem that to objects could have had the same Upload ID. To solve this problem the second catalogue of every pointing needed to be corrected for that, to prevent later confusions, resulting in strange proper motions. The next important column is the multi-frame ID, every measurement circle taken by VISTA has a unique identification number, so every detection with the same multi-frame ID was made under the same conditions like pointing and time. Only the particular detector could be different, but no source should be in two detectors and have the

⁴<http://space.ml/proj/GalaxyGAN>

same multi-frame ID. Each multi-frame ID corresponds directly to a single epoch later used in this thesis. To be able to use IRAF commands later, all catalogues needed to be split into smaller catalogues only containing data for one pointing, one detector and one epoch. At first, the filtering for epochs was done by utilising another column the Modified Julian Date (mjd), to do that all Modified Julian Dates had to be converted to an ordinal date and compared to a table provided by Maria-Rosa Cioni (appendix) to chose which epoch to take into consideration. Due to the nature of floating point numbers in Python, which are always rounded to one specific decimal place. This makes them a less suitable as filter criteria in that case since detections could slip in or out if the Modified Julian Date and the needed tolerance around that date were not chosen carefully. The better filter criteria proved to be the multi-frame ID. By just reading out all unique multi-frame IDs from the catalogues for every pointing in separate and checking them with the Archive Listing function⁵ at the VSA homepage, one can choose which multi-frame IDs to use for further calculations way clearer. To get a table one had simply to paste all unique multi-frame IDs into the form and to select the VMC as the survey. Multi-Frame IDs from the used catalogues, which did not show up in this table, refer to measurements, which are not released public jet. This sets of multi-frame IDs were then used to split the catalogues into single epochs. In addition to splitting the catalogues into even smaller ones containing only data from one type of objects, one pointing, one detector and one epoch, they were also filter based on the pperrbits column. Sources with a detection flagged with pperrbits higher than 256 were filtered out. This way those sources had been excluded from proper motion calculations, regardless of pperrbits of their other epochs. However, in the case of the galaxies, every detection with pperrbits smaller than 256 was used to match the epoch catalogues. The matching later found that the first epoch should be excluded too, which was due to high air mass, resulting in a fewer number of matches with other epochs. Next step was to check how the sources were distributed over each detector and if any trends in the distribution could affect the proper motion proper motion calculations. The next figure shows two pairs of corresponding epochs in 2D density maps. The right contains only galaxies, and the left only stars.

⁵horus.roe.ac.uk:8080/vdfs/VImageList_form.jsp

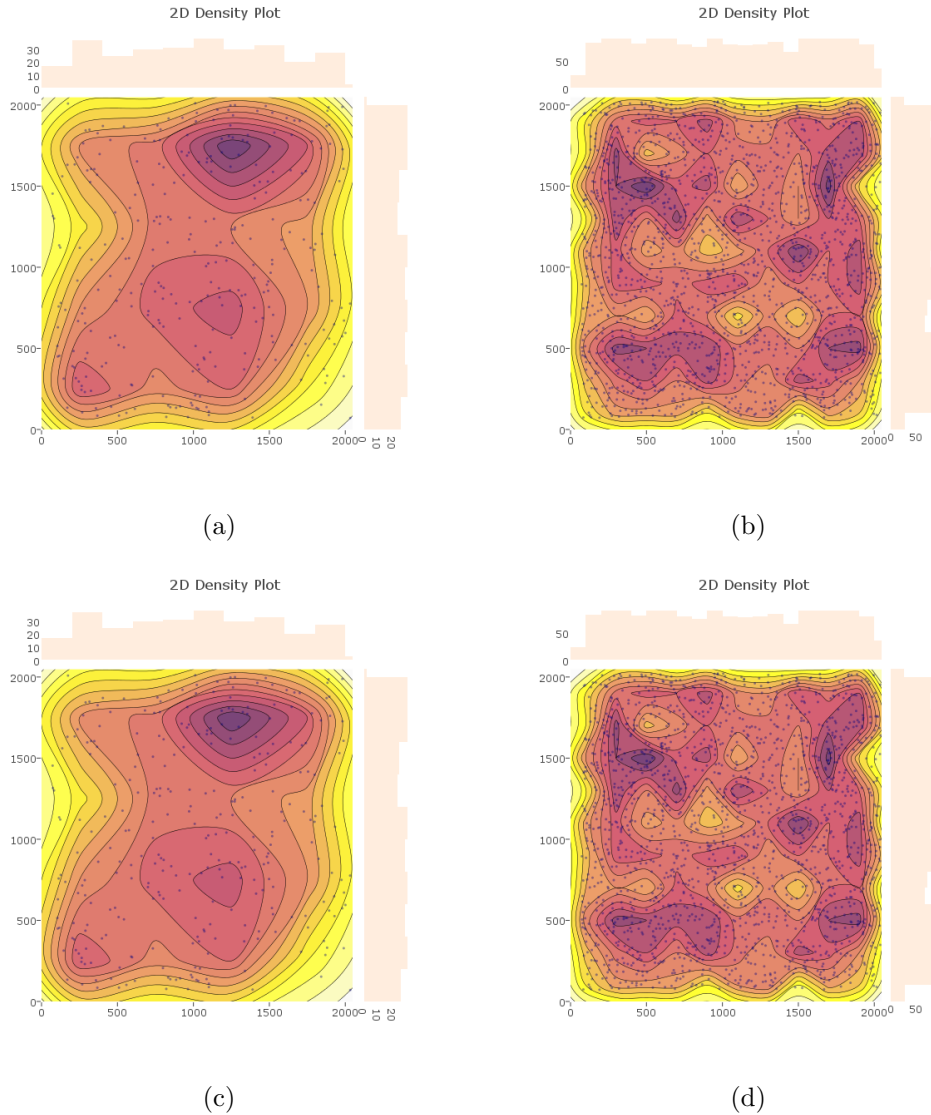


Figure 3: both figures show the the same reference epoch, the same detector and the same pointing

There are some effects that can be seen by comparing this figures. First galaxies and stars seem to be evenly distributed. There are some denser regions but do not vary much. Especially when regarding the histograms at the top and the right. One effect that is notable in these histograms are the edges. All epochs and all detectors show this behaviour this zone ist varies from detector to detector the following histograms 2D histogram show the same behaviour in that regard. Also when comparing dips and hills in the histograms on can see the that wherever the number of stars is higher where

the number of galaxies is mostly lower. This is due to the fact that denser regions contain more dust absorbing the light. The background galaxies should be evenly distributed. The next two figures show the distribution of galaxies first and that of stars after To get a better understanding of the distribution in whole. The detectors are ordered in the right sequence, and redder spots are more populated, but blue does not mean empty. as seen As seen in the density maps before is the detection of sources evenly distributed.

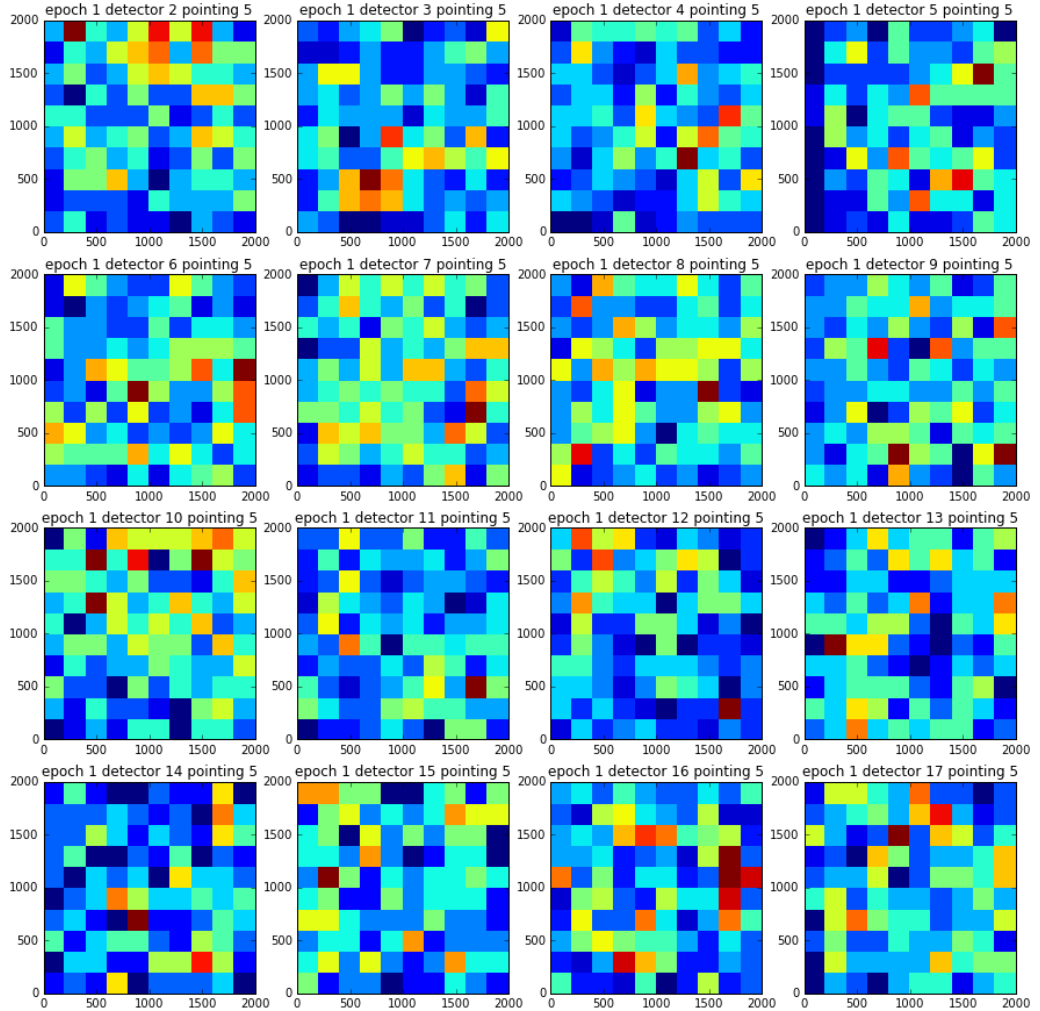


Figure 4: 2D histogram of galaxies

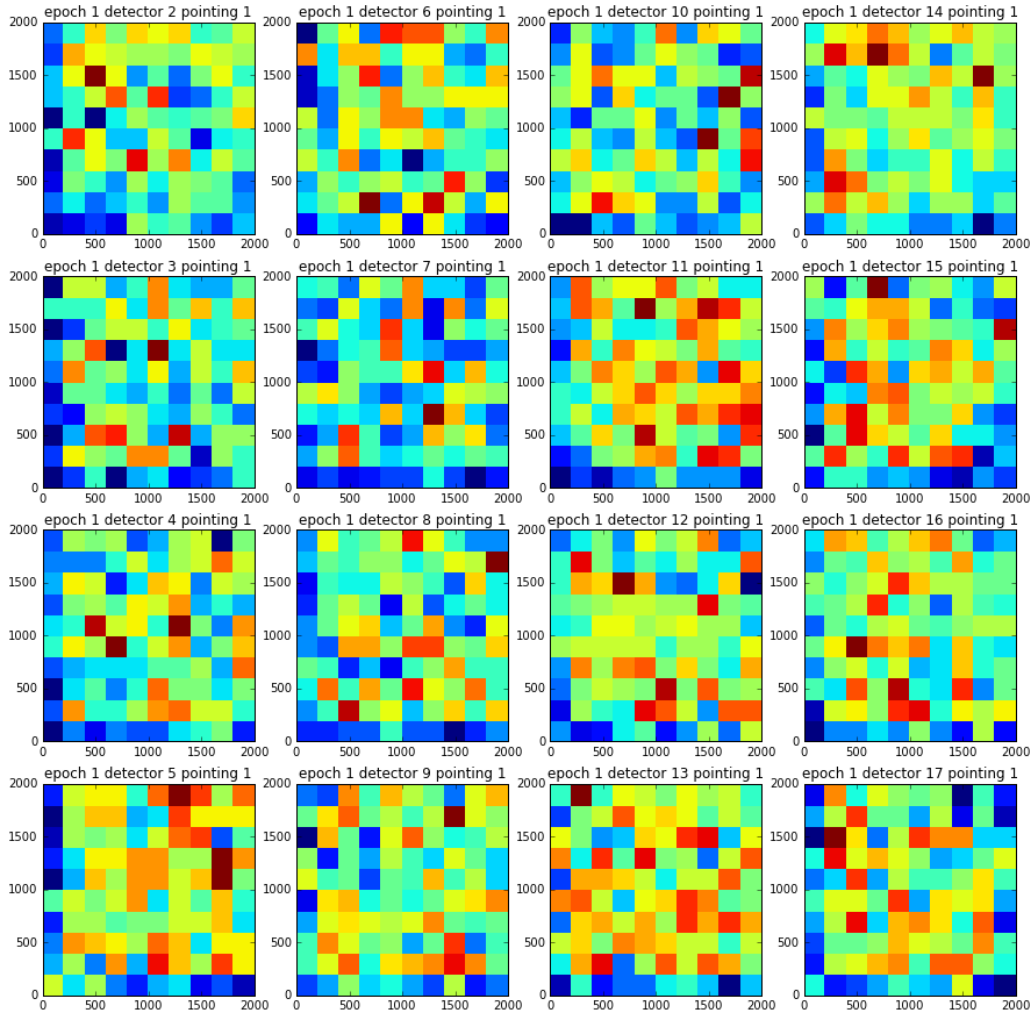


Figure 5: 2D histogram of stars

One can see that there are not significant differences in the distribution of galaxies nor stars within either type. Interesting to note is that wherever the density of stars gets lower the density of galaxies rises. This observation makes sense because higher dense regions contain more dust and reduced the brightness of objects behind. However, the overall densities were distributed evenly giving no hint of any predictable influences on the proper motion.

0.3 data processing

One of the main challenges was to structure the script in a way that is time and memory efficient. The catalogues were quite large and many data columns could not be dropped since they were needed in later steps. But the ability to drag additional data columns through the proper motion calculation showed to be beneficial later when selecting subsets and it showed to be easier to add additional data columns in early stages than later. Unwise scripting could easily result in ridiculous long calculation or completely fill the memory, what then again results in longer calculation times, if not overloading and thereby stopping the process. Working with this amount of data forces to be very cautious with calculation times, since every single calculation is potentially multiplied by a large number. Same goes for used memory. Cleverly placed loops, on the other hand, make it possible to repeat steps for different data sets automatically. The script is written to be able to run the whole calculation in one go if settings are chosen right and no errors occur or in steps chosen by the user. The file structure is done automatical, too. The Catalogues obtained by filtering and splitting were sorted by source type, pointing, detector and epoch, resulting in six pointings with 16 detectors each, every detector had ten epochs. Each epoch divided into two catalogues one for stars and one for galaxies. Galaxies and stars of the same epoch were tested to have the same multi-frame ID, to ensure that they are detected under the same conditions. The next calculation steps were done separately for every pointing and each detector following the method developed and published in Cioni et al. (2016).

0.3.1 astrometric reference frame

To derive proper motions, one needs an accurate reference frame. The measurements that were taken by VISTA were aimed at the same location by using a guide star catalogue. But this is not sufficient to get accurate proper motions since the displacements due to proper motions are way smaller than what can be achieved by precise aiming of a telescope. Based on the catalogues by calculation of the shifts between single epochs showed a scatter of up to 7 pixels in the CCD coordinate system, which converts 2,373 arcseconds at the sky. Proper motion displacements between two epochs in this thesis can be the order of 0.01 pixel or converted 0.003 arcseconds at the sky, thereby are much smaller than the average shifts between epochs. To measure these displacements an astrometric reference frame is needed. It was shown in the pilot study Cioni et al. (2014), that background galaxies can be used to derive reference frames for stars in the foreground. Background

galaxies are by far much further away than even the furthest stars used in this thesis, so their displacements due to their proper motions are very small compared to the displacements of stars in the foreground. The proper motion of the galaxies can be considered zero, in respect to the stars. One should note that proper motions derived in this thesis are absolute proper motions and are with respect to a seemingly non-moving astrometric reference frame obtained by using the background galaxies. The contribution of the three-dimensional space velocity of the solar system to that proper motion was not derived nor taken into account. However, when converting the proper motion into a two-dimensional space velocity tangential to the line of sight, this has to be done. As shown before, the galaxies were evenly distributed on each detector, with each detector having around 300 to 600 galaxies. Only one epoch had to be excluded, due to high airmass, that caused the number of galaxies to be way lower in that epoch than average. This led to lower matching numbers with this epoch, resulting in higher proper motion errors, since the reference frame was not accurate enough. Three IRAF tasks were used, to get the reference frame. IRAF is a general purpose software solution capable of reduction and analysis of astronomical data. To easier embed it into a Python code one had to use the Python package PyRAF as a tool for running IRAF tasks in a Python scripting language. The used IRAF commands are `xyxymatch`, `geomap` and `geotran`. They are sophisticated and fast tools often used in astronomy. Also, they are the main reason why the catalogues had to be split since using IRAF commands demands separate files. Future features of PyRAF could lead to eradicating that need, resulting in faster calculations. The first task, to be used, was `xyxymatch` on the galaxy catalogues. It matches two catalogues by using two coordinates, in our this case x and y coordinates on every detector. There were several settings to chose. The first setting is the matching mode there are modes to chose tolerance mode and triangles mode. Tolerance mode is a fast matching mode. Any initial transformation needed to be set in this tolerance mode were used as default. Meaning setting the linear transformation parameters described no initial movement, no initial rotation and an initial scaling of one. Separation was chosen to be zero since estimated shifts should be around zero. For the setting of tolerance, different numbers were tested. The tolerance determines in what limitation sources from both catalogues can be matched. A smaller number of 1-5 pixel resulted in a fewer number of galaxies getting matched, leading to bigger errors. Larger numbers like 10-20 pixel resulted in higher number of matches. However, later steps showed that the matching quality declined. 8-9 pixel delivered best results. For these catalogues. Using these settings some epochs could not be matched with some other epochs. By using different reference epochs, it was shown, that there were two groups

of epochs. Epochs of one and the same group could be matched fine with each other, but not with the other group. Testing those matches with higher tolerances ≥ 15 pixels resulting in some matches. Larger shifts⁶ in x and y coordinates seemed to be the case. Since these shifts were unknown to that point, the other matching algorithm was tested. The "triangles" mode does not require any knowledge of an initial linear transformation. This mode is computationally expensive. The settings for this mode were chosen, to reduce the chance sources getting incorrectly matched. To test this configuration, both matching modes were compared by matching multiple different epochs. The parameters used were changed to result in matching the same galaxies over a variety different matches. With a difference, that a single matching takes far more time in triangle mode to be derived. Some matches took up to five minutes and more depending on the size of both catalogues. This resulted in very long calculation times with all 6 pointings times 16 detectors and 9 epochs to match to one reference epoch for each detector. Thanks to multiprocessing this was reduced to roughly one day. The matching derived by the triangular mode presented shifts as high as 15-18 pixel in x coordinates and 20-23 pixel in y coordinates. Tests showed a limit to possible shifts using these settings. This limit was found to be around 25 pixels. Matching Catalogues with larger shifts did not deliver matches. However, the obtained shifts matching the catalogues should not have been in the data since the aiming of the VISTA telescope should be within a much smaller error and info from the headers of the original fits files suggested no methodical changes in the observations. Like a change in the used guide stars or a change in the pattern in which different the pointings were taken. It was found out in the VISTA VIRCAM news listing⁷ that on the 21st of August 2010 a "horizontal re-centering of VIRCAM" took place. Every epoch before that date is shifted by around 15 pixels in x and 20 pixels in y to epochs taken later. With this knowledge, every affected matching pair can be corrected by adjusting the linear transformation parameters in the matching mode settings. That made it possible to use the faster tolerance mode again. The next step in the calculation was using the IRAF geomap, which computes a transformation to fit two catalogues together by using the matching catalogue calculated by IRAF xyxymatch. The IRAF geomap task was done in double precision for the coordinate transformation calculations. It was possible to evaluate matchings directly after that calculation. The quality criteria for good matchings in was seen in the xrms and yrms values. A good matching had rms values lower than 0.2. Every match with rms values < 0.3 was regarded as bad matching

⁶Example xyxymatch in the appendix

⁷<https://www.eso.org/sci/facilities/paranal/instruments/vircam/news.html>.

and was either way rematched in triangular mode or was discarded and not used in further calculation. The average rms value was 0.21. There was a correlation between the number of galaxies being matched. Higher matching number led to smaller rms values. To be sufficient, there was a need for around 250 matches to be found. Matchings with up to 600 found matching galaxies had rms values as low as 0.16.

Table 1: table xrms and yrms of pointing 1 epoch for all detectors

detector	matches	xrms	yrms
2	469	0.19	0.21
3	403	0.20	0.19
4	389	0.25	0.23
5	366	0.21	0.22
6	360	0.19	0.18
7	425	0.21	0.20
8	363	0.17	0.17
9	495	0.21	0.19
10	483	0.20	0.19
11	318	0.22	0.23
12	357	0.22	0.21
13	393	0.19	0.18
14	269	0.24	0.22
15	512	0.23	0.21
16	385	0.24	0.22
17	354	0.19	0.26
average	372.25	0.21	0.21

As shown in the table above and below do the average of all xrms and yrms values was found to be 0.21. Which is not only the average of those list but fits very good with every random sample of rms values. The last IRAF command to be used was IRAF geotran. It was used in the next step to transform the catalogues for all epochs all detectors and all pointing except the reference epochs. This transformation was done by using the transformations derived by IRAF geomap. Every epoch with the same pointing and same detector was now transformed into the same reference frame. IRAF geotran transform based on 6 values it shifts, scales and rotates based on 6 values gained from IRAF geomap⁸.

⁸Example IRAF geomap file in the appendix

Table 2: table xrms and yrms of pointing 1 and detector 2

epoch	matches	xrms	yrms
1	469	0.19	0.21
2	521	0.17	0.18
6 3	454	0.27	0.23
4	508	0.18	0.20
5	454	0.24	0.24
6	441	0.21	0.22
7	445	0.21	0.21
8	518	0.20	0.18
9	497	0.19	0.18
average	371.67	0.21	0.21

0.3.2 using the closest galaxy as reference

In early stages of this thesis, there was the idea to test a method used in Casetti-Dinescu et al. (2016) [6]. The main idea is to use the stars as a reference system and to calculate the proper motion of the closest galaxies to each star. This would compensate for more effects caused by the detector on a small scale since the reference is located more closely compared using the whole detectors as a reference frame. There were some tests on some epochs. However, this was not possible at that time. The stars were supposed to be used as the reference system and there were big shifts in coordinates in the catalogues. Since the cause of these shifts was unknown at that time, any matching would have had unacceptable calculation times in triangular mode due to the higher number of stars compared to the number of galaxies. Tolerance mode was proven to be inaccurate and unable to find the correct matchings. The matching tolerance used in Casetti-Dinescu et al. (2016) was 1 arcsecond, that would mean less than 3 pixels in on the VIRCAM. A similar matching tolerance was not close to being able to produce any results. Due to a lack of time this method had then to be abandoned. With the cause of these shifts now being known continuing would be possible.

0.4 proper motion calculation

In order to calculate the proper motions, the reference epochs were joined with all transformed epoch catalogues of the same pointing and same detector by using the numerical python rec function *join_by* with the upload ID used as the key. This procedure was fast and has the bonus effect that sources that were not present in all epochs were automatically filtered out, but requires all upload IDs to be unique to work properly. These resulting catalogues contained the unique upload ID, detector, the x and y coordinates for every epoch for every source, the Modified Julian Date of every epoch and some other data columns. Since only VISTA data of epochs measured in K filter was used, it was necessary to also join catalogues with additional data about the magnitudes over K and J-K for every source. To plot colour-magnitude diagrams. These magnitude catalogues were provided by Prof. Cioni. With these magnitudes, there was an additional column added, which flagged every source with a colour-magnitude diagram region. These Regions were defined in Cioni et al. 2013. They correspond to different stellar populations with different stellar ages. The classification was done by using the following Table taken from the pilot study.

Table 3: Stellar populations (table taken from Cioni et al.2013)

Region	Boundaries		log(Age)(yr)	MW %
A	$K_s < 19$ $K_s > 7.5 \cdot (J - K_s) + 16.5$	$(J - K_s) > ?0.2$ $K_s < ?25 \cdot (J - K_s) + 16.5$	$LMC7.95 \pm 0.27$	0
B	$K_s < 19$ $K_s > 3.333 \cdot (J - K_s) + 16.5$	$K_s > -25 \cdot (J - K_s) + 16.5$ $K_s < -13.333 \cdot (J - K_s) + 19$	$LMC8.51.16$	0
C	$K_s < 19$ $K_s < -6 \cdot (J - K_s) + 19.9$	$K_s > -13.333 \cdot (J - K_s) + 19$ $K_s > -13.333 \cdot (J - K_s) + 19$	$LMC8.87 \pm 0.14$	1
D	$K_s < 19$ $K_s > -2.5 \cdot (J - K_s) + 18.5$	$K_s > -6 \cdot (J - K_s) + 19.9$ $K_s < -15 \cdot (J - K_s) + 25$	$LMC9.19 \pm 0.14$	2
E	$16 < K_s < 19$ $K_s > -15 \cdot (J - K_s) + 25$	$K_s < -30 \cdot (J - K_s) + 37$	$LMC9.53 \pm 0.36$	0.3
F	$K_s < 19$ $K_s > -30 \cdot (J - K_s) + 37$	$(J - K_s) < 0.9$ $K_s > -8.75 \cdot (J - K_s) + 22.125$	$LMC9.81 \pm 0.19$	94
G	$12.5 < K_s < 16$	$0 < (J - K_s) < 0.2$	$LMC8.13 \pm 0.10$	13
H	$12.5 < K_s < 16$ $K_s < -15 \cdot (J - K_s) + 22$	$(J - K_s) > 0.2$	$LMC9.75 \pm 0.76$	77
I	$K_s > 12.5$ $K_s > -15 \cdot (J - K_s) + 22$ $K_s < -15 \cdot (J - K_s) + 25$	$(J - K_s) > 0.4$ $K_s < -9.167 \cdot (J - K_s) + 20.917$	$LMC8.61 \pm 0.17$	15
J	$(J - K_s) > 0.4$ $K_s < -2.5 \cdot (J - K_s) + 18.5$	$K_s > -9.167 \cdot (J - K_s) + 20.917$ $K_s < -15 \cdot (J - K_s) + 25$	$LMC9.15 \pm 0.60$	1
K	$12.5 < K_s < 16$ $K_s < -8.75 \cdot (J - K_s) + 22.125$	$K_s > -15 \cdot (J - K_s) + 25$	$LMC9.45 \pm 0.37$	3
L	$12.5 < K_s < 19$ $K_s > -8.75 \cdot (J - K_s) + 22.125$	$0.9 < (J - K_s) < 2.2$	Galaxies	3

Also, added was a column noting with pointing every source detection was part of. All the galaxy catalogues were stacked, the same was done

separately for the star catalogues, resulting in two large catalogues. The next table shows the number sources gained by this procedure and the counts for individual populations. The Sources that did not get flagged with a specific colour-magnitude diagram region from A to L, also went through the proper motion calculation for the sake of completeness but were ignored in later calculations. Except for the galaxies were all galaxies were used to calculate the median proper motion.

Table 4: counts of different populations in field LMC8_8

population	number
A	1190
B	4436
C	6813
D	12538
E	34053
F	21152
G	102
H	3901
I	9275
J	41958
K	12952
L	1189
None	5140
Stars	154699
Galaxies	26896

0.4.1 proper motion galaxies

At first, the proper motions of the galaxies were derived. They were calculated by using a linear least square fit for x and y coordinates separately and the corresponding Modified Julian Dates for every single source. The slope of this fit was the proper motion in units of pixel per day. The results for the galaxies were tightly centred around 0. Some sources showed abnormally high proper motion. By checking the individual coordinates of every epoch for those sources, it could be shown that some displacements seemed to be out of place, seemingly occurring by just being mistaken upload IDs or random errors in x or y coordinates. Being only a tiny fraction of the larger number of samples in whole they were simply filtered out. The next figure shows the proper motion distribution of galaxies gained by this procedure.

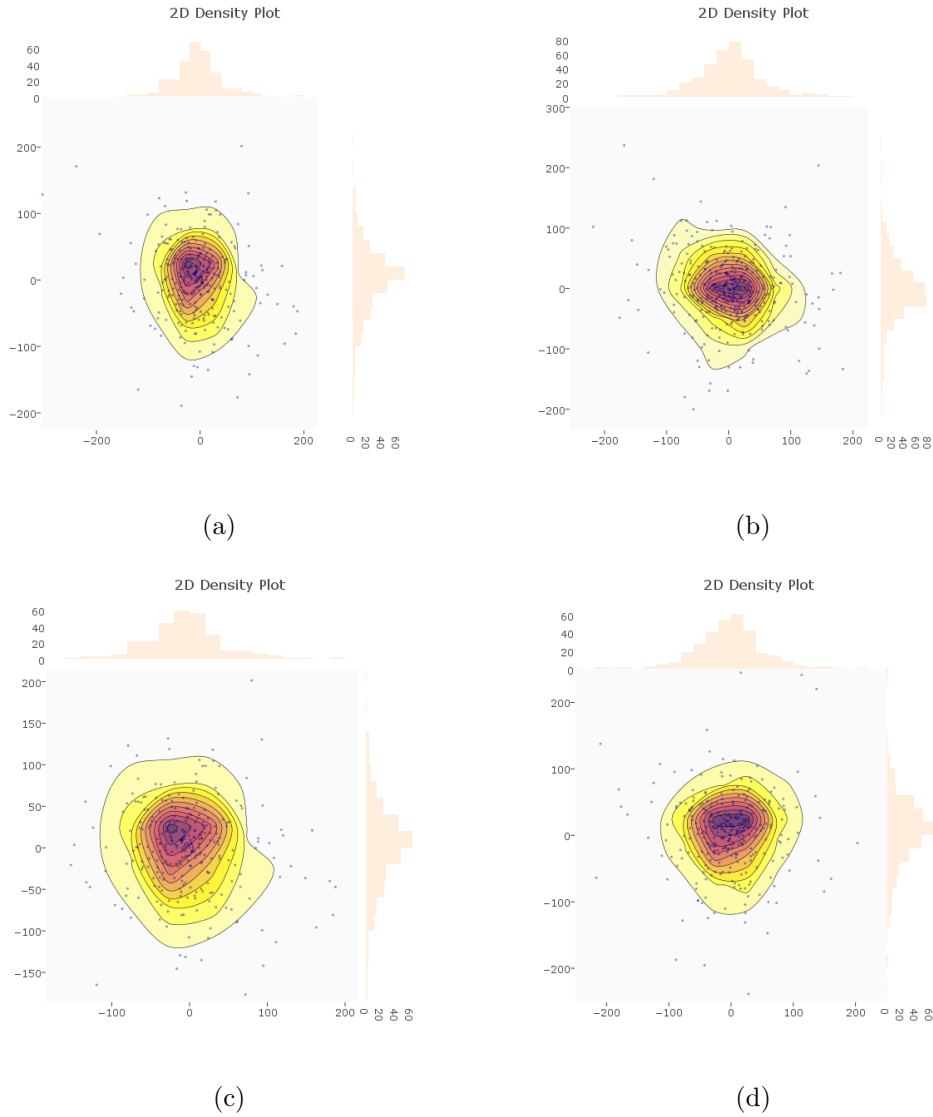


Figure 6:

Whenever the number of matching galaxies for one of the epochs was too small (less than 100), it could be directly seen in this proper motion distribution. Then they were not be centred around zero any more and the shape would get more irregular. The Histograms show a Gaussian distribution in both directions.

0.4.2 proper motion conversion

Next step was to convert the proper motions from units of pixel per day into units of milliarcseconds per year. They were multiplied by 365.25 corresponding to the number of days of a year. To convert the pixel into milliarcseconds, the CD matrix parameters from the headers of the paw prints were used. Only the headers of the reference epochs had to be used since they already represented the reference frame. Also, all detectors of the same epoch shared the same needed parameters, leading to one set of parameters per pointing. These sets contained the multi-frame ID of the reference epoch, to ensure that conversion was done with the right parameters for each source. Also, they contained the parameters CRP1X1 and CRP1X2 representing the centre of the paw print and the CD matrix containing $CD_{1,2}$ and $CD_{2,1}$. The equations used in Cioni et al. 2016 were utilised as well.

$$\xi = CD_{1,1}(x - CRP1X1) + CD_{1,2}(y - CRP1X2) \quad (1)$$

$$\eta = CD_{2,1}(x - CRP1X1) + CD_{2,2}(y - CRP1X2) \quad (2)$$

The first derivatives were derived from those equations since the proper motion in pixel per day was the slope of the linear least square fit, also being the first derivative of a linear function. Thus only $CD_{1,2}$ and $CD_{2,1}$ were needed using the following equations for every source of the catalogue, with dx and dy being the proper motions in x and y coordinates gained from the linear least square fit.

$$d\xi = (CD_{1,1}dx + CD_{1,2}dy) \cdot 3.6 \cdot 10^6 \quad (3)$$

$$d\eta = (CD_{2,1}dx + CD_{2,2}dy) \cdot 3.6 \cdot 10^6 \quad (4)$$

The factor $3.6 \cdot 10^6$ was used to convert from degree to milliarcseconds. Outliers were removed by using a three sigma clipping on the gained galaxy proper motion catalogue. The Sigma was calculated by using the median absolute deviation.

0.4.3 The median absolute deviation

The median absolute deviation (MAD) is often used in statistics to give a robust estimate[7] a for the standard deviation. The main reason it was used here, was that it is very resilient to outliers. It is defined as,

$$MAD = median(|X_i - \bar{X}|) \quad (5)$$

Using the median absolute deviation avoids any usage of calculating a mean(μ) as used in the formula for the standard deviation(σ) which is influenced by outliers.

$$\sigma = \sqrt{\frac{1}{N} \sum_{i=1}^N (x_i - \mu)^2} \quad (6)$$

For symmetric Gaussian distributions, a relationship between standard deviation and median absolute deviation can be estimated by,

$$\sigma \approx 1.4826 \cdot MAD \quad (7)$$

The standard deviation was then used to exclude galaxies further away than 3σ from the median. This was repeated until no galaxies were removed anymore. Then the median proper motion for the galaxies was calculated in units of milliarcseconds per year. Since the proper motion results correspond to the reference frame, so do $d\nu$ and $d\eta$ correspond directly to $\mu_\alpha \cos \delta$ and μ_δ . The median proper motion of galaxies was checked for any trends in regarding the detectors.

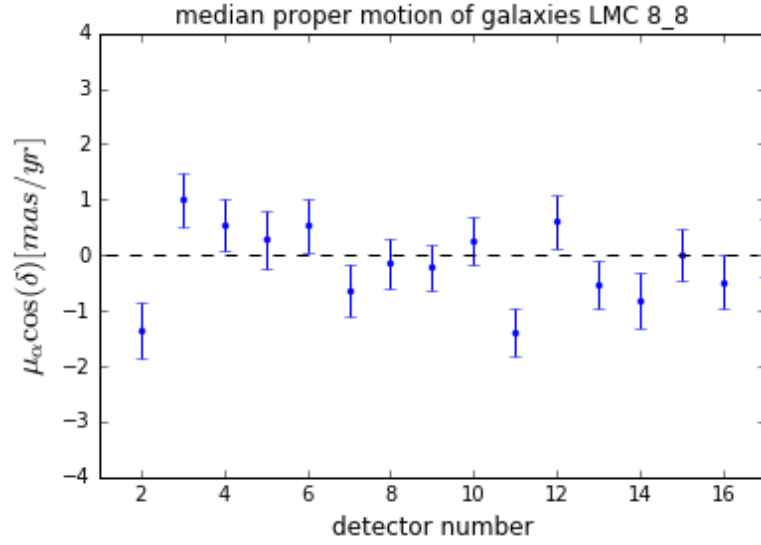


Figure 7: median proper motion $\mu_\alpha \cos \delta$ of galaxies on detector basis

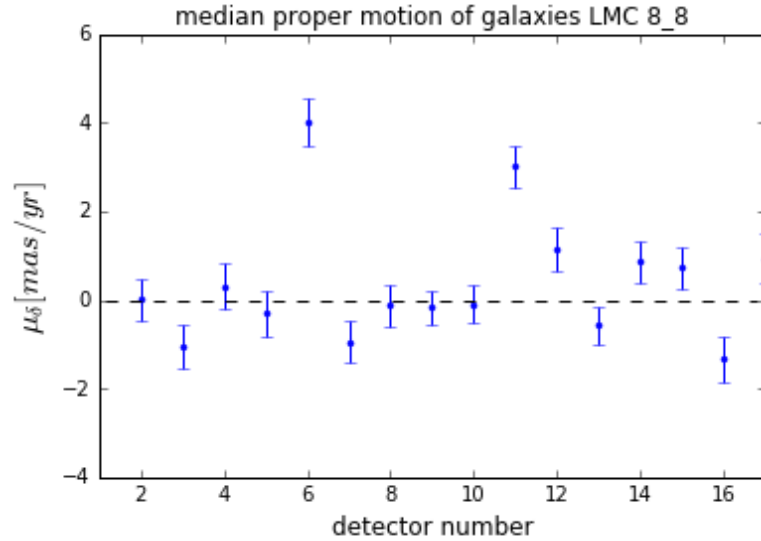


Figure 8: median proper motion μ_δ of galaxies on detector basis

As shown in the figures above all median proper motions were consistent with zero. This fact was expected since the galaxies should not move at all. Any of their movement is an effect of a systematic residual, which needs to be adjusted when calculating the median proper motions of the star populations. Only detector number 15 deviates from the others. However, this detector is known to have less quality. As mentioned before any poor matching would

lead larger median proper motions. This made these plots a useful tool to easily find a poor matching in the 864 matching catalogues produced by xyymatch. The median proper motion for all galaxies resulted in $\mu_\alpha \cos \delta = -0.49 \pm 0.13 \text{ mas/yr}$ and $\mu_\delta = 0.1 \pm 0.13 \text{ mas/yr}$. Comparing the result with the median proper motions of the galaxies from both previous studies and the other fields STR11 and STR21 shows, that proper motion calculations on detector-by-detector basis give better results. Since the galaxies should not have any proper motions at all, any discrepancy should be independent of the field observed mainly only the method used, sample sizes and the way the centres of the galaxies were determined should play a role. One can see that larger sample sizes result in smaller median proper motions of the galaxies.

Table 5: median proper motion of galaxies in all three fields

field	N	$\mu_\alpha \cos \delta$ [mas/yr]	σ_μ [mas/yr]	σ [mas/yr]	N	μ_δ [mas/yr]	σ_μ [mas/yr]	σ [mas/yr]
LMC8.8	25079	-0.49	0.14	22.17	25031	0.10	0.14	22.15
STR1.1	31532	0.38	0.10	17.46	31562	0.03	0.10	17.12
STR2.1	30720	-0.41	0.06	10.80	30235	0.04	0.06	10.45

0.4.4 proper motion stars

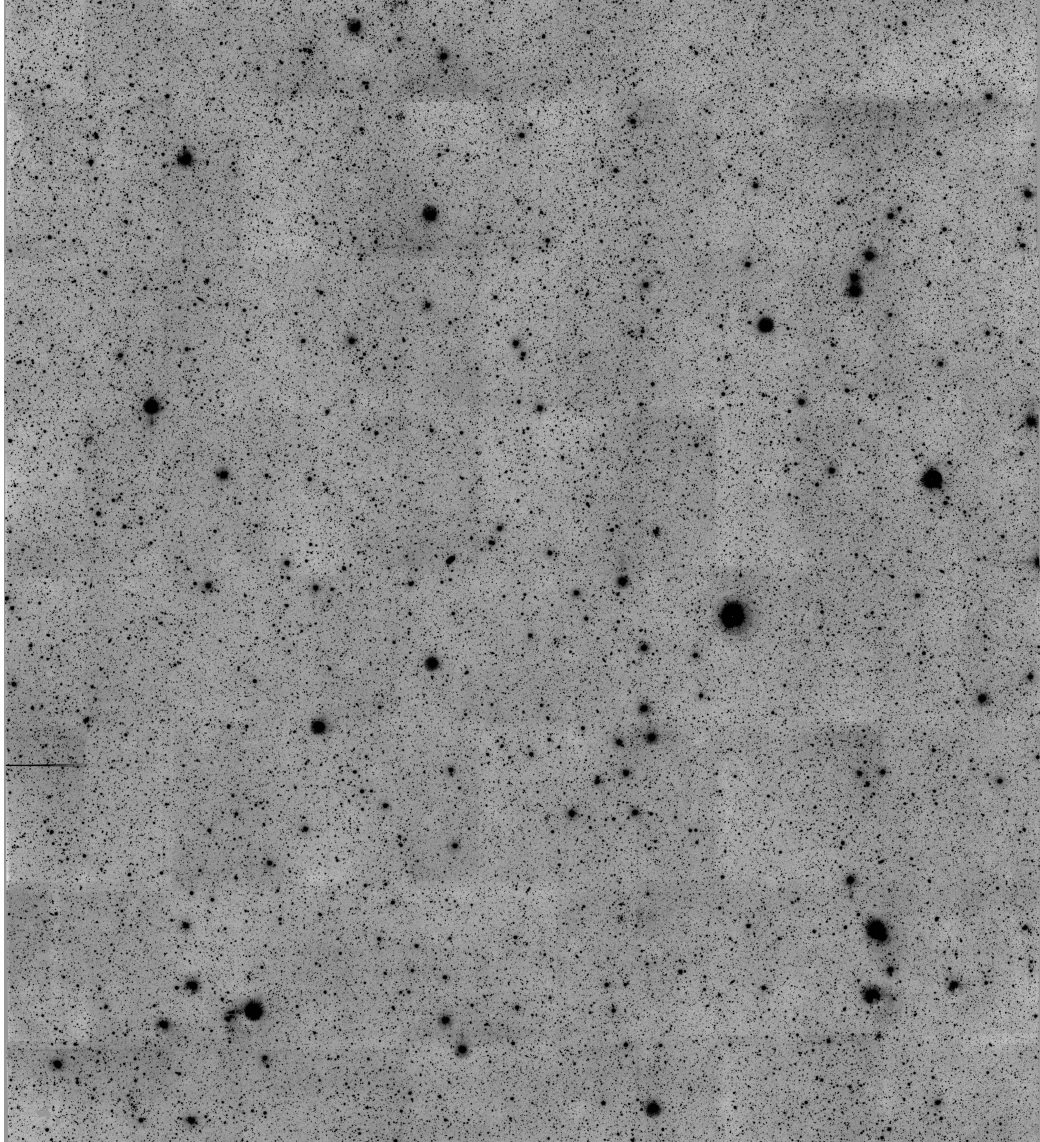


Figure 9: star field LMC 8.8 from VSA

The proper motion calculation of the stars was done analogue to the calculation of the galaxies. First, the star catalogues gained by splitting as described in the sample selection were transformed by using IRAF `geotran` and the transformation derived by IRAF `geomap` with the galaxies to adjust them the reference frame of the galaxies. The next step was again to join the catalogues of all epochs by their upload ID and adding the K and J-K

magnitudes provided for the stars. The stars were then flagged with regions based on their K and J-K magnitudes as shown below.

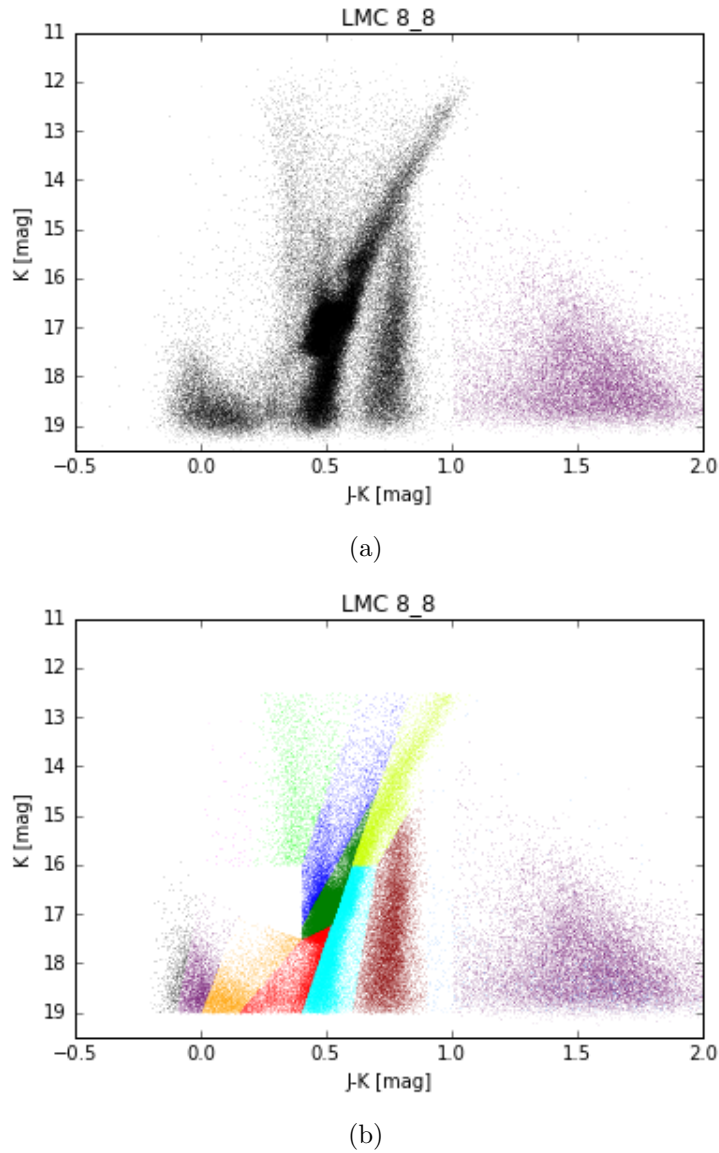


Figure 10: (a) colour magnitude diagram of stars in LMC 8_8; (b) colour magnitude diagram of populations in LMC 8_8

All catalogues were stacked and the proper motion was derived for every source using the same linear least square fit, described in the proper motion calculation of the galaxies. The next figures show a plot this fit for four randomly chosen star.

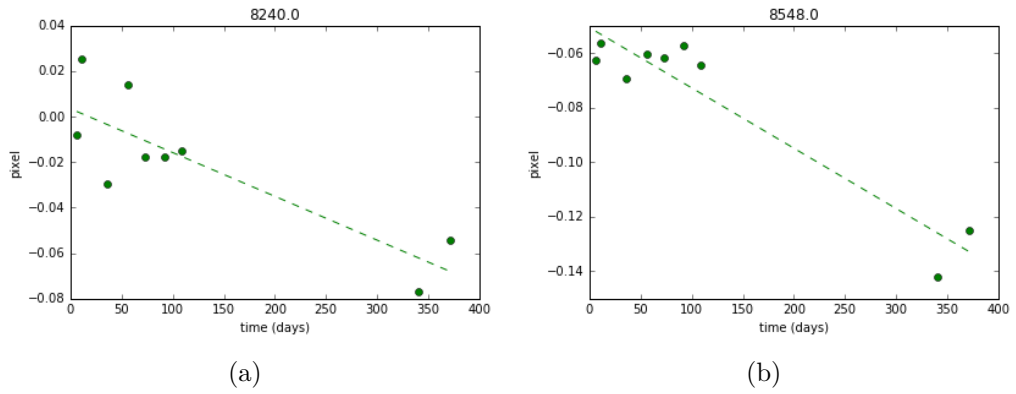


Figure 11: random sources with linear least square fit

The gained proper motions were then converted to milliarcseconds per year. The next plots show the proper motion as a function of K magnitude and J-K magnitudes. They show the same features as shown in the pilot study.

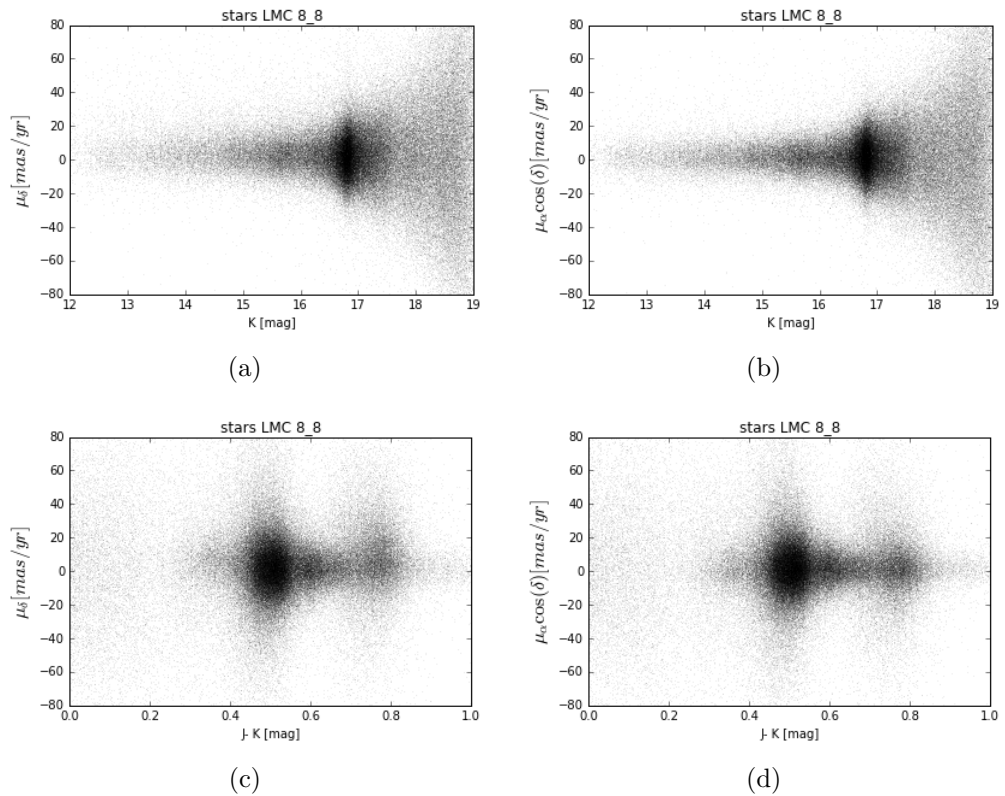


Figure 12:

The next step was to calculate the median proper motions for every population defined earlier. A subset was selected based on the flag classified by the K and J-K magnitudes, selected earlier. This subset then was sigma clipped analogue to galaxies. The median proper motions were then corrected for the median proper motion of the galaxies, to compensate for the systematic residual, found earlier. The next table and figures shows the corrected median proper motions for field LMC 8.8.

Table 6: proper motion of population LMC 8.8. corrected for galaxy proper motion

population	$\mu_\alpha \cos \delta$ [mas/yr]	σ [mas/yr]	N	σ_μ [mas/yr]	μ_δ [mas/yr]	σ [mas/yr]	N	σ_μ [mas/yr]
A	1.15	24.79	1074	0.76	1.27	27.16	1087	0.82
B	1.64	33.91	4025	0.53	3.25	35.36	4030	0.56
C	2.18	35.28	6157	0.45	1.67	37.33	6195	0.47
D	2.30	25.32	11144	0.24	1.44	25.3	11116	0.24
E	2.589	16.64	28843	0.1	1.68	17.95	29090	0.11
F	2.73	16.99	18259	0.13	7.96	20.21	18553	0.15
G	3.13	9.55	93	0.99	4.31	8.77	90	0.92
H	1.90	7.94	3543	0.13	6.96	9.99	3517	0.17
I	1.98	8.18	8313	0.09	2.71	9.57	8269	0.11
J	2.14	11.11	38042	0.06	1.57	11.85	37811	0.06
K	2.09	6.92	11584	0.06	2.15	8.36	11320	0.08
L	0.98	33.71	1071	1.03	4.63	43.46	1099	1.31
LMC	2.20	6.91	77303.0	0.02	1.68	7.65	78151	0.03
Galaxies	-0.49	37.93	25079	0.14	0.10	36.82	25031	0.14

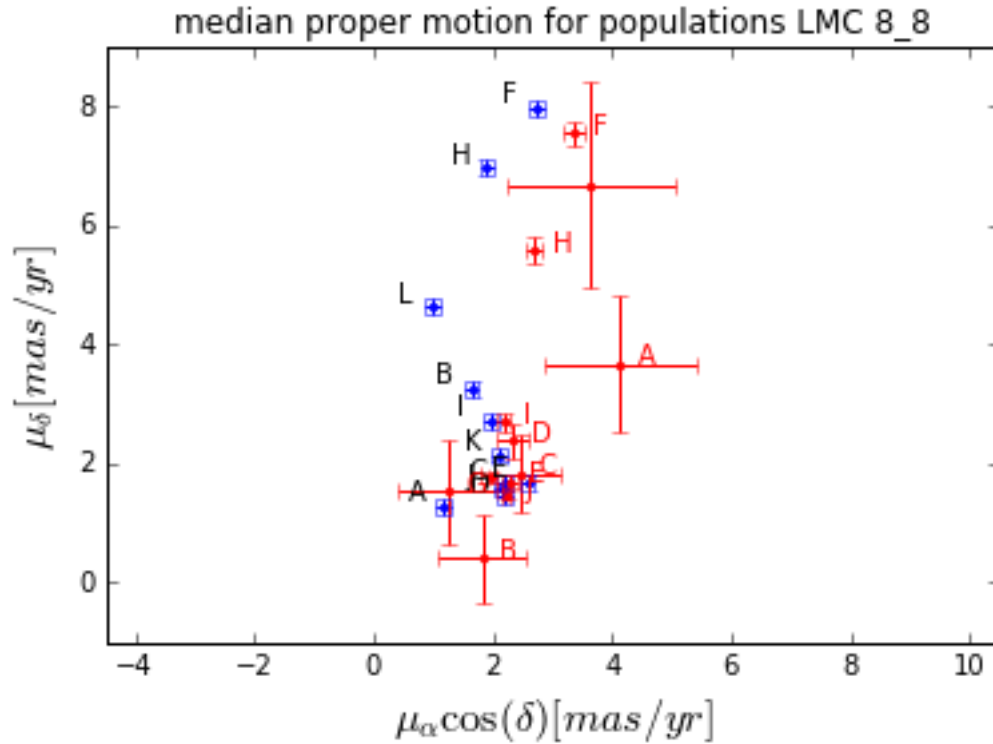


Figure 13: LMC 8-8 proper motion of stellar populations compared to Cioni at al. (2014)

The red points show the proper motion with corresponding errors derived in Cioni at al.(2014). To compensate for any residuals the median proper motion of all galaxies sigma clipped was subtracted from the median proper motions of every stellar populations. The second plot shows a small area of the first plot, to better differentiate between populations.

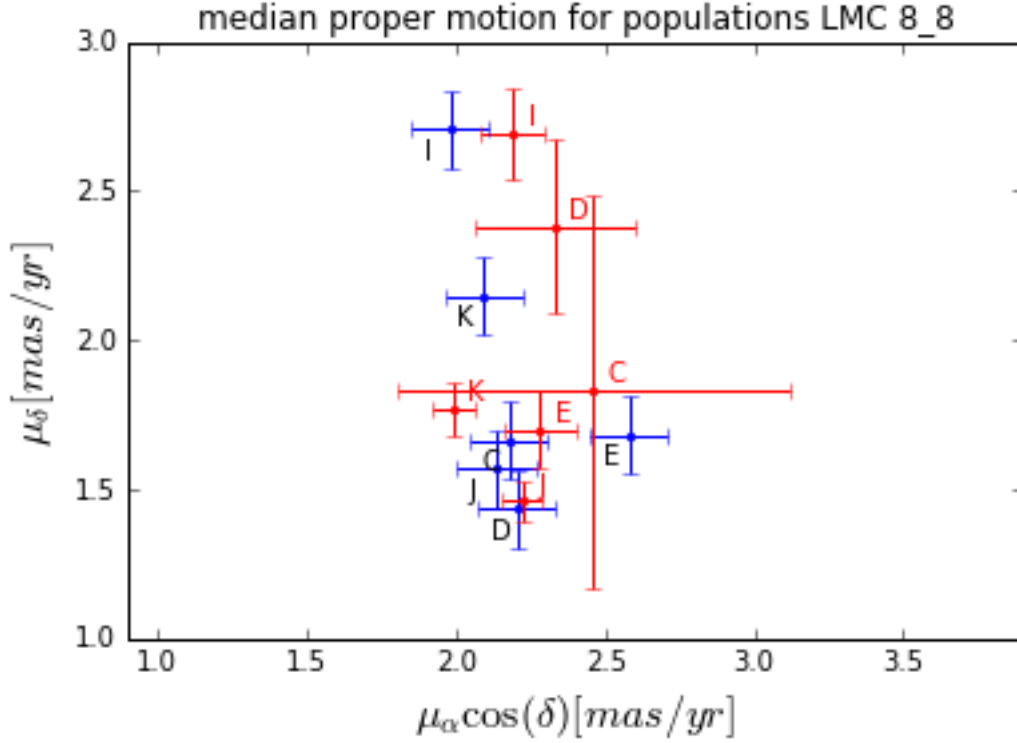


Figure 14: LMC 8.8 proper motion of stellar populations associated with the Large Magellanic Cloud compared to Cioni et al. (2014)

One can easily see, that some proper motions cluster at one spot of the diagram, while the others are clearly separated from them and mainly on a higher proper motion at least in one axis. Those populations were assumed to be associated with the Large Magellanic Cloud. Proper motions of populations with large error bars, are to be neglected since their counts are too small to be reliable.

0.4.5 proper motion LMC stars

To calculate an average proper motion of stars associated with the Large Magellanic Cloud. A subset of all stars was chosen to only contain to assumed populations. The populations used were C, D and J. This subset was then again sigma clipped. Resulting in a proper motion, that was then again corrected to compensate for the median proper motion of the galaxies.

The median proper motion for LMC stars resulted in $\mu_\alpha \cos \delta = 2,20 \pm 0.16 \text{ mas/a}$ and $\mu_\delta = 1.68 \pm 0.17 \text{ mas/a}$.

The next plot shows the sigma clipped subset(left) in comparison to the

rest of the stars (right). In mid one can see sigma clipped subsets of assumed populations divided into subsets based on K magnitude.

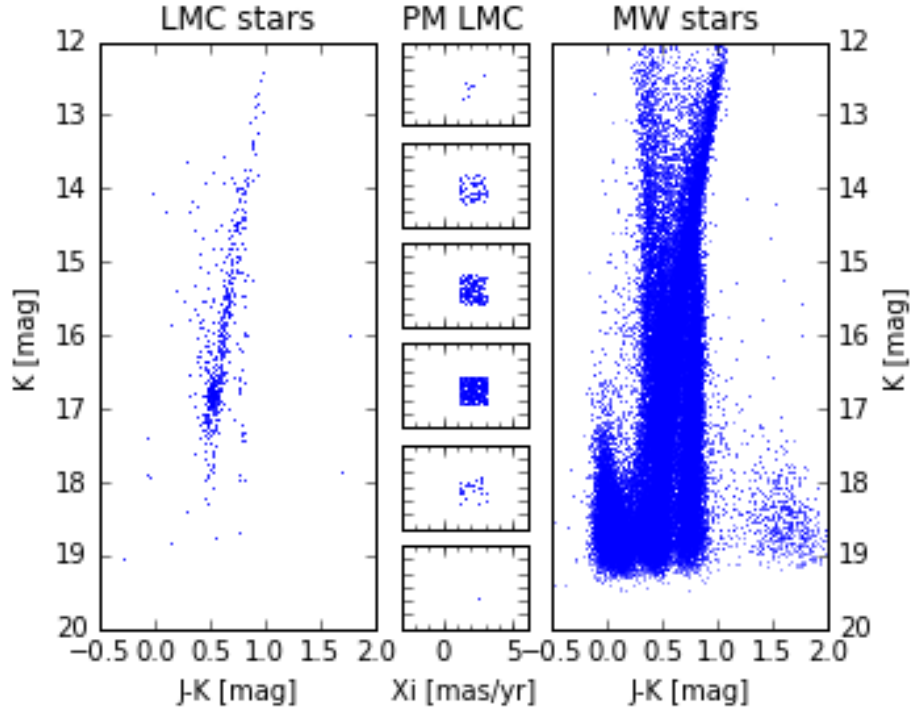


Figure 15: LMC 8.8 proper motion selection

0.4.6 errors

Calculation of proper motions is always difficult. There are lots of errors that can be considered like seeing, ground-based telescopes are heavily affected by seeing. That is why most telescopes are built on mountains like VLT and VISTA. But as shown even earlier even that benefit is not enough. As shown with the epoch that was had to be excluded due to the high air mass. Usually one needs to carefully error propagate for example include the error of the pixel or errors that are intrinsically part of the CCD as seen in the histograms that show, that the edges of the detectors are not as good as the centres at working. In this thesis, most of the errors are of simply systematic nature the fact the galaxies do not move at all compared to the foreground in solid. VISTA main advantage is the sheer number of sources, due to the large field of view. Most single measurements are not even close to being reliable. That is why the median absolute deviation was used to give an estimate of the error. The statistical error for the galaxies was then added as

the systematic error. This error is by far dominating all other error sources. But doing the calculation on a detector-by-detector basis shows to be more reliable.

0.5 proper motion results

Comparing the proper motion to previous measurements shows to be very consistent with Cioni et al.(2013)[4]. The following table. Shows some comparisons.

Table 7: proper motion LMC field 8.8

Author	year	$\mu_\alpha \cos \delta [mas/yr]$	$\mu_\delta [mas/yr]$
thesis		$2,20 \pm 0.16$	1.68 ± 0.17
Cioni	2013	2.20 ± 0.35	1.70 ± 0.36
Pedreros	2011	2.1 ± 0.2	1.5 ± 0.2

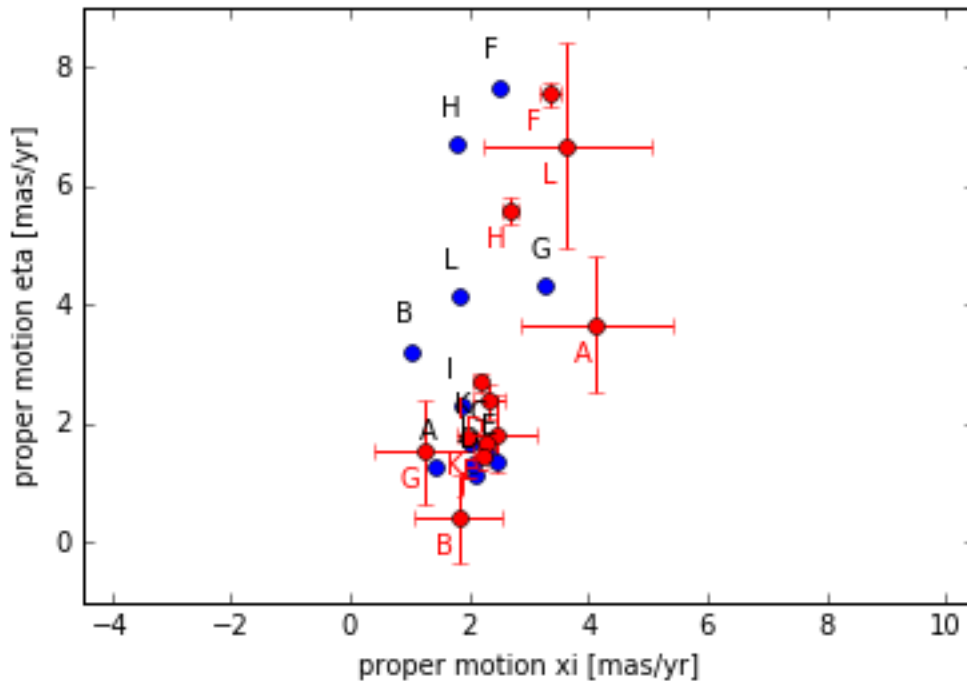


Figure 16: PM LMC 88

0.6 proper motion centre of mass

As described in van der Marel and Cioni et al.(2001)[8] is the Large Magellanic Cloud assumed to be of a disk-like shape. In the outer regions of the LMC were many pieces of evidence found to confirm that. The next picture shows a depiction of that. Two angles describe, how this disk is placed in three-dimensional space on a viewing line. Those angles were defined as i and Θ . With i being an inclination on the south-north axis with $i = 0$ meaning face-on view and $i=90$ meaning edge-on view. Θ was defined as the position angle on the east-west axis measured from west to east. There are many different estimations for those angles, depending on the method used to determine them. Later comparisons are made with proper motion calculations observed by the Hubble Space Telescope(HST) and published in van der Marel et al.(2013)[9]. It would be just logical to use $i = 39.6 \pm 4.5$ and $\Theta = 147.4 \pm 10.0$ determined by HST with proper motion measurements. To get an idea of how the LMC is aligned a disk model was plotted into a 3D-diagram.

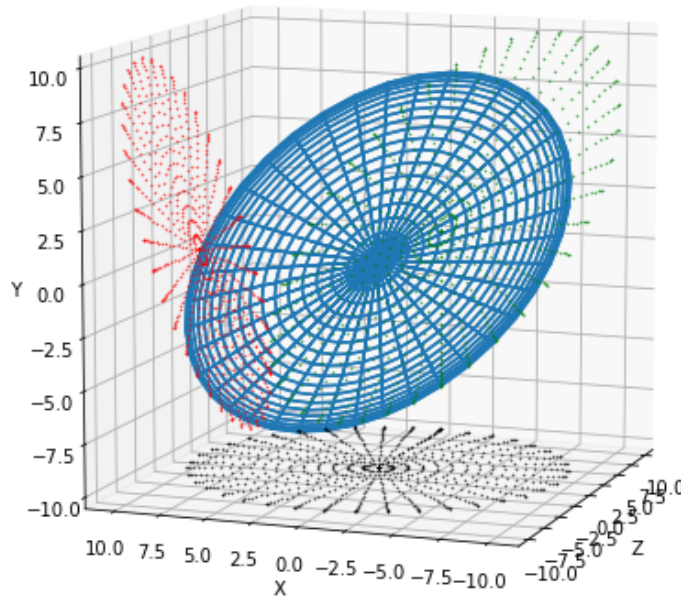


Figure 17: simple disk model LMC

The idea of this chapter is to correct the measured proper motion of LMC 8.8 for the effect caused by changing the viewing angle to get the proper motion that would be measured at the centre of the Large Magellanic Cloud. The next to pictures are taken from van der Marel et al.(2002) was used to be understood the problematic.

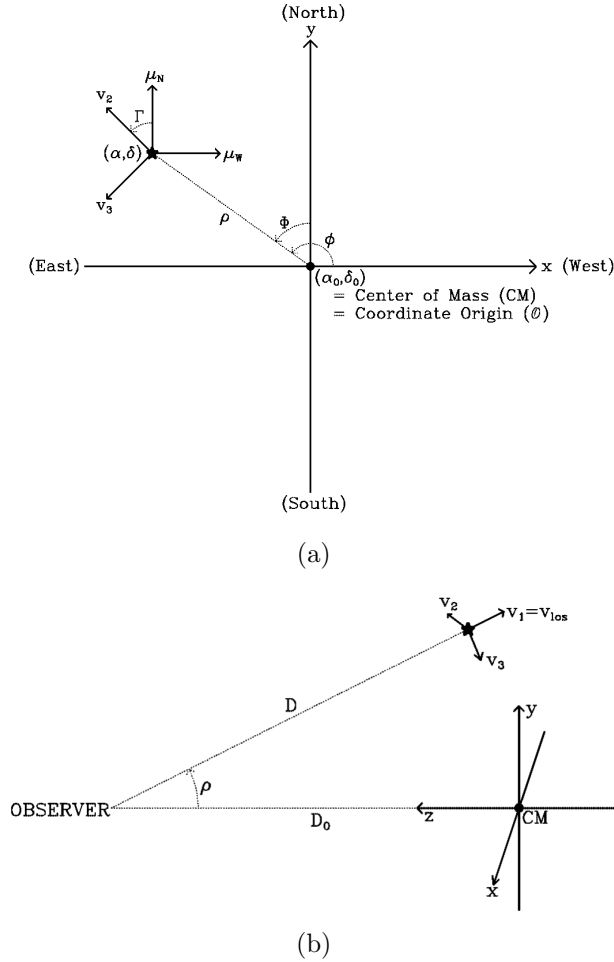


Figure 18: (a) shows the front view with the observer looking at the centre of mass (centre of the disk); (b) shows the side view.

One should realise that the proper motions $\mu_\alpha \cos \delta = 2, 20 \pm 0.17 \text{ mas/yr}$ and $\mu_\delta = 1.68 \pm 0.16 \text{ mas/yr}$ measured with field LMC 8.8 are not aligned to the x and y -axis in side view figure. They belong to the plane spanned by v_2 and v_3 . Also is it not possible to calculate v_1 with the VISTA catalogues since proper motions only measure velocities perpendicular to the line of

sight. With spectra would it be possible to calculate a radial velocity by using the Doppler effect, for example, 4MOST data in the future.

$$\mu_W = -(d\alpha/dt) \cos \delta, \mu_N = d\delta/dt \quad (8)$$

with the right ascension α and declination δ , this leads as described in van der Marel et al.(2002) to,

$$\mu_W = \frac{\cos i \cos \rho - \sin i \sin \rho \sin(\phi - \theta)}{D_0 \cos i} \cdot (-\sin \Gamma \nu_2 - \cos \Gamma \nu_3) \quad (9)$$

$$\mu_N = \frac{\cos i \cos \rho - \sin i \sin \rho \sin(\phi - \theta)}{D_0 \cos i} \cdot (\cos \Gamma \nu_2 - \sin \Gamma \nu_3) \quad (10)$$

with,

$$\cos \rho = \cos \delta \cos \delta_0 \cos(\alpha - \alpha_0) + \sin \delta \sin \delta_0 \quad (11)$$

$$\sin \phi = \frac{-\cos \delta \sin(\alpha - \alpha_0)}{\sin \rho} \quad (12)$$

and

$$\cos \Gamma = [\sin \delta \cos \delta_0 \cos(\alpha - \alpha_0) - \cos \delta \sin \delta_0] / \sin \rho \quad (13)$$

$$\sin \Gamma = [\cos \delta_0 \sin(\alpha - \alpha_0)] / \sin \rho. \quad (14)$$

The first part of the following table was created by the usage of needed values taken from the table 1 in van der Marel et al. (2014). The values used were taken from the model that was fitted to proper motions measurements. The table also contains values known about field LMC 8.8 such as the centre coordinates and the proper motion that was calculated before.

$$\Theta = \theta - 90^\circ \quad (15)$$

Table 8: values for centre of mass proper motion calculation

	van der Marel 2014	LMC 8.8	unit
i	39.6 ± 0.25		deg
Θ	147.4 ± 10		deg
D_0	50.1 ± 2.5		kpc
α_0	78.76 ± 0.52		deg
δ_0	769.19 ± 0.2		deg
$\mu_\alpha \cos \delta$		$2, 20 \pm 0.16$	mas/yr
μ_δ		1.68 ± 0.16	mas/yr
α		78.76	deg
δ		766.25	deg

This led to $\mu_W = -1, 92 \pm 0, 2$ and $\mu_N = 0.10 \pm 0.2$ using the proper motion . The first Component matches quite nice with the $\mu_{PM,W} = 1.91 \pm 0.02$ and the second lies with $\mu_N = 0.229 \pm 0.047$ within the error.

The following two figures show two set of stars chosen by sigma clipping in the first are possible LMC stars. One can see that they are moving all similar in the same direction. This movement is mainly, due to the the moment of the whole LMC system only a small fraction is rotation. There was no gradient to be found. Which makes also sense due to the fact that LMC 8.8 is in the outer region of the LMC and the rotation curve is assumed flat there.

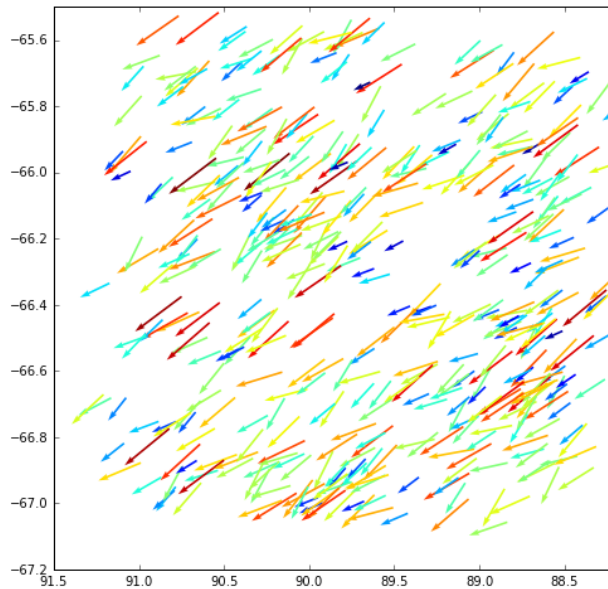


Figure 19: vector field LMC

The second picture shows a set of possible Milky way foreground stars.

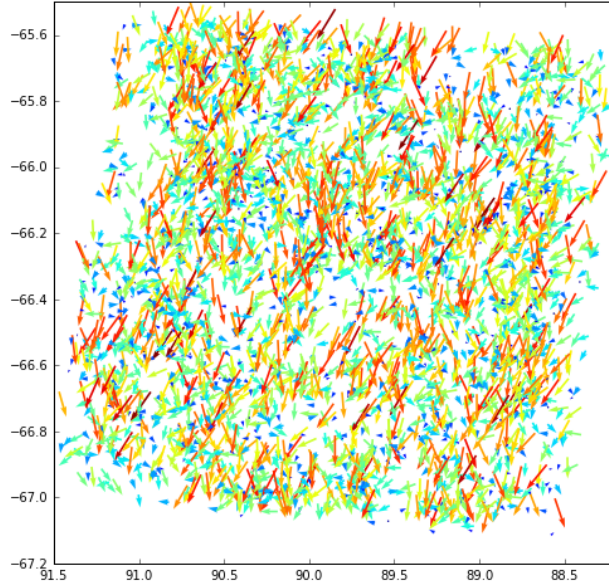


Figure 20: vector Milky way stars

0.7 VMC stream fields

0.7.1 STR 1_1

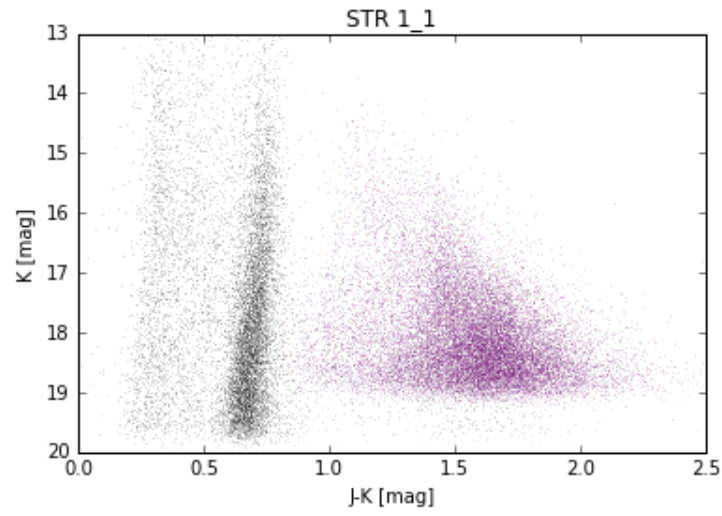
Stream field STR 1_1 was the first field to test the code further. Fewer stars were contained in the provided catalogues. However, the number of stars was larger, then in LMC 8.8. The first step was then to filter all unique multi-frame IDs from the catalogues of each point and to check with the VSA which multi-frame IDs to use. The pick for the reference epoch was sadly lucky chosen. Only one of 10 epochs was affected by a large shift in x and y coordinates, and it happened to be the chosen reference epoch. For the matchings, every setting was chosen as in LMC 8.8. Since there were nearly no other shifts between the other epoch. Every other match found by xyymatch showed the same result. That lead to finding the reason of the unexpected shifts earlier found. The next epoch in the timeline was taken right in the night after the VIRCAM was recentred on 21th of August 2010. To confirm that finding IRAF xyymatch was tested in tolerance mode, with an initial shift of -15 pixel in x and -21 pixel in y. The matching then went fine. IRAF geomap then found only small shifts, probably due to aiming at with 2-3 pixel. That made it possible to calculate the average. The good

aiming of the rest of the epochs made it possible to get a good estimate for the shift due to the recentring of VIRCAM. The rest of the proper motion calculation was done automatical by the script. The only thing that had to be changed was how the populations were marked. The way the colour-magnitude diagram regions defined earlier had to be adjusted, due to the fact that most stars in STR 1_ were further assumed to be further away. Since the stream fields seemed to be closer to the SMC both the K and the J-K magnitude were justed, to compensate for the reddening due to the further distance. The values used for this were taken from Cioni et al. 2015(cite), $K = +0.6$ and $(J - K_s) = -0.04$. This resulted in the following counts for both fields. They were assumed to be sufficient, for further use.

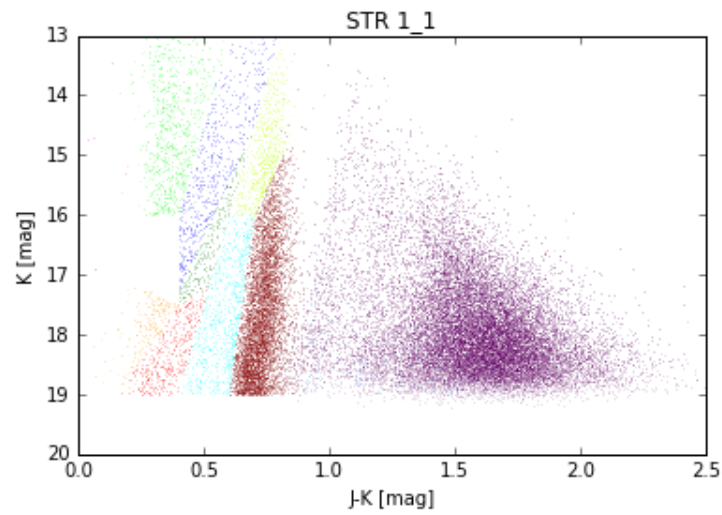
Table 9: counts of sources of fields STR 1_1 and STR 2_1

population	number STR 1_1	number STR 2_1
A	2	1
B	7	6
C	346	474
D	754	917
E	1361	1819
F	10246	8821
G	11	19
H	1320	1350
I	985	979
J	402	378
K	1114	1136
L	279	290
None	3894	5683
Stars total	20721	21873
Galaxies	33707	40182

The next two figures show by how far the number of galaxies dominated the number of stars. These fields seem to be an optimal environment for further developing the method, that had to be abandoned. The number of stars is tall enough to provide a good reference frame, but not as tall as in LMC 8_8 and the epochs seemed to be without significant disturbing shifts except the one epoch.



(a)



(b)

Figure 21: (a) colour magnitude diagram of stars in STR 1_1; (b) colour magnitude diagram of populations in STR 1_1

The rest of the proper motion calculation in STR 1_1 was done analogue to LMC 8.8 without any problems, except that some populations had to be excluded from the calculation due to a lack of members, resulting in the following table.

Table 10: proper motion of population LMC 8.8. already corrected for galaxy proper motion

population	$\mu_\alpha \cos \delta$ [mas/yr]	σ [mas/yr]	N	σ_μ [mas/yr]	μ_δ [mas/yr]	σ [mas/yr]	N	σ_μ [mas/yr]
A	4.30	2.05	2	1.45	2.41	0.17	2	0.12
B	2.81	14.32	5	6.48	3.71	4.99	5	2.23
C	4.22	8.50	332	0.47	0.39	8.50	333	0.47
D	5.60	10.93	722	0.41	0.69	12.23	733	0.45
E	5.77	9.01	1248	0.26	2.37	9.32	1253	0.26
F	5.95	10.58	9777	0.11	4.30	11.41	9786	0.12
G	3.57	6.13	10	1.94	2.27	3.23	8	1.14
H	5.54	6.27	1247	0.18	3.37	7.07	1247	0.20
I	5.26	6.26	880	0.21	2.99	7.46	904	0.25
J	5.58	6.53	376	0.34	3.06	8.29	380	0.43
K	5.83	10.86	1035	0.34	5.09	13.20	1038	0.41
L	0.20	10.83	245	0.69	1.58	11.42	249	0.72
Galaxies	0.38	17.46	31532	0.10	0.03	17.12	31562	0.03

When comparing these proper motion one can easily see that they spread. With to two groups being more stacked. They seem to be somewhere close to LMC and SMC proper motions but can not be directly associated with either one. Also, there are some uncertainties due to small populations. But the script still finds a spread and proved to be working.

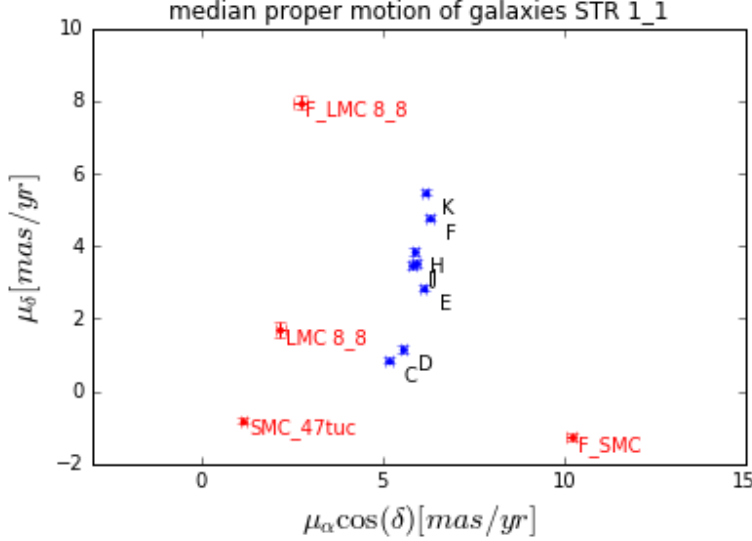


Figure 22: median stars STR11 compared to proper motions from other fields

0.7.2 STR 1_1

Since the reason for the big shifts was known when calculating this field's proper motion no problems in matching occurred. While these epochs were not as good aligned as *STR1_1*. The only thing that changed was that the upload IDs for the galaxies had to be corrected like the upload IDs of the stars in LMC 8.8 since the number of galaxies in the original catalogues was larger than the limit of the VSA supplies in a single catalogue. The other calculations were then done analogue to LMC 8.8 and STR 1₁. The population counts were similar to *STR1_1*, but the proper motions are quite far from everything else. So it was not possible to see any interesting relevance in these numbers. The only fact is that they are far spread.

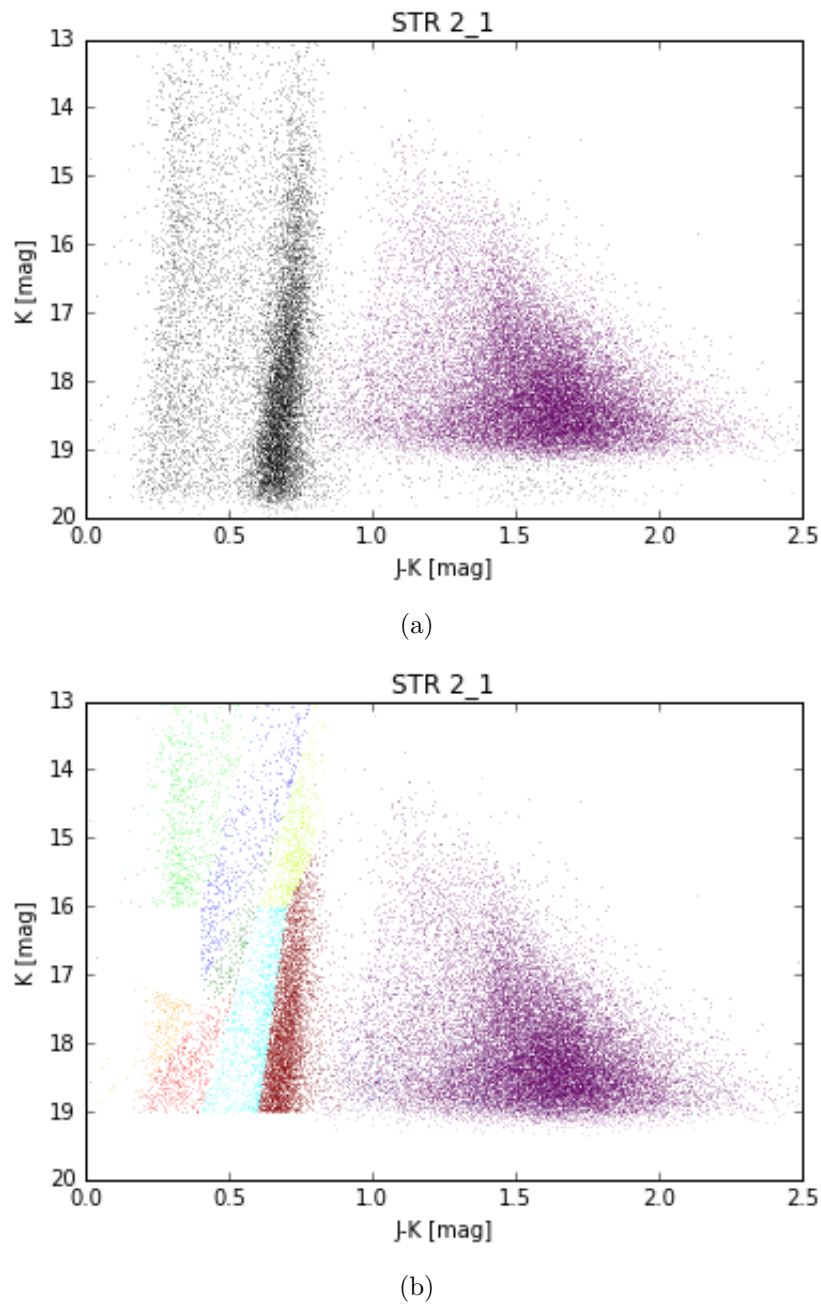


Figure 23: (a) colour magnitude diagram of stars and galaxies in LMC 2.1; (b) colour magnitude diagram of populations in LMC 2.1

Table 11: proper motion of population STR 2.1.

population	$\mu_\alpha \cos \delta$ [mas/yr]	σ_μ [mas/yr]	σ [mas/yr]	N	μ_δ [mas/yr]	σ_μ [mas/yr]	σ [mas/yr]	N
C	3.57	5.76	409	0.28	-4.74	5.95	412	0.29
D	4.68	7.80	798	0.276	-6.10	7.00	770	0.25
E	7.75	6.83	1442	0.18	-4.23	6.28	1405	0.17
F	8.07	7.80	7449	0.09	-2.65	6.43	7286	0.08
H	6.61	5.06	1107	0.15	-2.13	3.92	1146	0.16
I	7.22	4.46	682	0.17	-2.53	4.53	779	0.16
J	4.97	4.33	312	0.24	-2.63	4.29	331	0.24
K	10.99	9.03	952	0.29	-2.85	6.24	940	0.20
L	1.06	7.67	230	0.51	-0.81	4.92	186	0.36
STR2.1	-0.41	10.80	30720	0.06	0.04	10.45	30235	0.06

The next figures show those proper motions comparing them with results from LMC field 8.8 and the proper motion results of the SMC from Cioni et al. 2015. The proper motion of the Milky way stars from the field LMC 8₈ and were for comparison

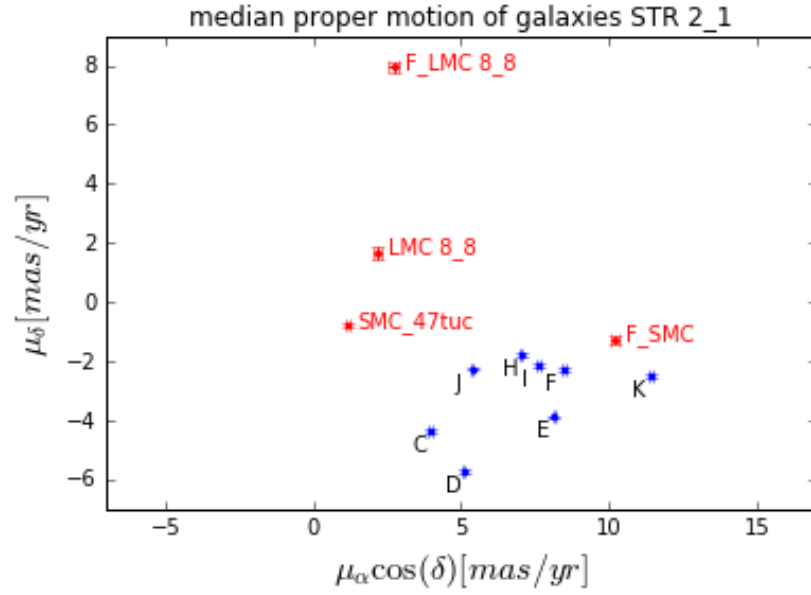


Figure 24: median stars STR 2.1 compared to proper motions from other fields

0.8 conclusion

The proper motions calculated in this thesis were consistent with previous investigations, for example, Cioni et al.(2013). The developed Python code was shown to be sufficient, in proper motion calculation using VMC data. It was possible to improve on the results of median proper motions for different populations in field LMC 8_8 and in addition, proper motions could be derived for some populations in the two stream fields STR 1.1 and STR 2.1. The code showed that it could produce results even with unintended and unexpected shifts as large as 23 pixels in one coordinate, making it still reliable. Using this script enables to calculate proper motions efficiently and mainly automatically. The method used here and developed in Cioni et al. 2016 was shown to work in the outer disk of the LMC as well as in the less populated stream fields. Improvements in differences in median proper motions between different populations could also be determined by smaller systematic errors. And stream field STR 1.1 shows potential benefits when it comes to test the method used by Casetti-Dinescu et al.(2016)[6] with VMC catalogues.

0.9 future

There are many opportunities to continue this work in the future. The straightest step would be to run the script on some additional fields in the LMC, to get a two-dimensional velocity field, which could lead depending on the accuracy to a rotation curve. But the most recent opportunity would be cross-matching VMC data with Gaia data to further improve the accuracy of the proper motion calculation by extending the baseline. Gaia is able to deliver highly accurate measurements of positions. It would be interesting to see how the results turn out with higher accuracy. Also, some new quasars were found behind the Magellanic clouds. Investigations in this direction could lead to an improvement of the reference frames since quasars are more qualified as reference points since they are pointier sources than the spatially extended galaxies. Since, VISTA is fast at surveying the Magellanic Clouds, due to its large field of view, a higher accuracy could lead the way to better an understanding of the Clouds and their internal kinematics. Therefore calculating more LMC fields with greater precision could narrow down where to find the gravitational centre of the LMC and to answer the question where to look for a central black hole. With this inside into the kinematics of LMC and SMC many uncertainties about them could be finally figured out, and detailed models about their star formation history and chemical abundance could be tested. Also having large accurate proper motion catalogues of the Clouds observed by VISTA will be useful by the time 4MOST starts its deep survey of the Magellanic Clouds. The spectral data and therefore the resulting line of sight velocities will be useful to create three-dimensional velocity maps and 3D-models of the Magellanic Clouds that will benefit many fields of modern astrophysics significantly. However, line of sight velocities tend to have lower uncertainties than proper motions that means such 3D-models would improve by reducing the proper motion uncertainties.

0.10 acknowledgment

I want to thank everyone who supported during my studies and endured listening to me, while I was happily talking endlessly about physics. Also, I want to thank the AIP especially Maria-Rosa for giving me this great opportunity to work on such an interesting thesis. And many thanks to the Magellanic Clouds group and the Milky way and local volume group for the interesting inputs and for being so friendly.

The things I learned in writing this thesis will surely be beneficial to my future, since the world is getting more and more dominate by large quantities of data, as used in this thesis.

sincerely thank you.

0.10.1 Eidesstattliche Erklärung

Ich versichere, dass ich die vorliegende Diplomarbeit ohne fremde Hilfe angefertigt und keine anderen als die angegebenen Quellen und Hilfsmittel benutzt habe. Alle Teile, die wörtlich oder sinngemäß einer Veröffentlichung entstammen, sind als solche kenntlich gemacht. Die Arbeit wurde noch nicht veröffentlicht oder einer anderen Prüfungsbehörde vorgelegt.

Potsdam, den

Unterschrift

Bibliography

- [Maj+10] Daniel J. Majaess et al. “Anchoring the Universal Distance Scale via a Wesenheit Template”. In: (July 14, 2010). arXiv: 1007.2300v2 [astro-ph.GA].
- [Tan+14] Jonathan C. Tan et al. “Massive Star Formation”. In: (Feb. 5, 2014). DOI: 10.2458/azu_uapress_9780816531240-ch007. arXiv: 1402.0919v3 [astro-ph.GA].
- [Cio+17] Maria-Rosa L. Cioni et al. “Pulsating stars in the VMC survey”. In: (Mar. 20, 2017). arXiv: 1703.06769v1 [astro-ph.GA].
- [Cio+13] M. -R. L. Cioni et al. “The VMC survey -IX. Pilot study of the proper motion of stellar populations in the LMC from 2MASS and VISTA data”. In: (June 18, 2013). DOI: 10.1051/0004-6361/201322100. arXiv: 1306.4336v2 [astro-ph.GA].
- [Sut+14] Will Sutherland et al. “The Visible and Infrared Survey Telescope for Astronomy (VISTA): Design, Technical Overview and Performance”. In: *A&A* 575, A25 (2015) (Sept. 16, 2014). DOI: 10.1051/0004-6361/201424973. arXiv: 1409.4780v2 [astro-ph.IM].
- [CG16] Dana I. Casetti-Dinescu and Terrence M. Girard. “Proper Motion of the Draco Dwarf Galaxy from Subaru Suprime-Cam Data”. In: (June 3, 2016). DOI: 10.1093/mnras/stw1337. arXiv: 1606.00977v1 [astro-ph.GA].
- [PH01] T. Pham-Gia and T.L. Hung. “The mean and median absolute deviations”. In: *Mathematical and Computer Modelling* 34:7-8 (Oct. 2001), pp. 921–936. DOI: 10.1016/s0895-7177(01)00109-1.
- [MC01] Roeland P. van der Marel and Maria-Rosa L. Cioni. “Magellanic Cloud Structure from Near-Infrared Surveys. I. The Viewing Angles of the Large Magellanic Cloud”. In: *The Astronomical Journal* 122.4 (Oct. 2001), pp. 1807–1826. DOI: 10.1086/323099.

- [MK13] Roeland P. van der Marel and Nitya Kallivayalil. “Third-Epoch Magellanic Cloud Proper Motions II: The Large Magellanic Cloud Rotation Field in Three Dimensions”. In: (May 20, 2013). DOI: 10.1088/0004-637X/781/2/121. arXiv: 1305.4641v1 [astro-ph.CO].

List of Figures

1	VMC coverage map green marked fields were used in this thesis. The figure was taken from VMC ESO Phase 3 Data Release Description	7
2	VISTA telescope with VLTs in the background (Photo credit: G.Hudepohl / ESO taken from Sutherland et al. 2015)	8
3	2D density maps	11
4	2D histogram of galaxies	12
5	2D histogram of stars	13
6	proper motion galaxies LMC8_8	21
7	median proper motion $\mu_\alpha \cos \delta$ of galaxies on detector basis	24
8	median proper motion μ_δ of galaxies on detector basis	24
9	star field LMC 8.8 from VSA	26
10	Colour magnitude diagrams LMC8_8	27
11	proper motion LMC8_8	28
12	Colour magnitude diagrams LMC8_8	28
13	LMC 8.8 proper motion of stellar populations compared to Cioni et al. (2014)	30
14	LMC 8.8 proper motion of stellar populations associated with the Large Magellanic Cloud compared to Cioni et al. (2014)	31
15	LMC 8.8 proper motion selection	32
16	PM LMC 88	33
17	simple disk model LMC	34
18	schematic views taken from Marel et al.(2002)	35
19	vector field LMC	37
20	vector Milky way stars	38
21	Colour magnitude diagrams STR 1_1	40
22	median stars STR11 compared to proper motions from other fields	41
23	Colour magnitude diagrams STR2_1	43
24	median stars STR 2.1 compared to proper motions from other fields	44

List of Tables

1	table xrms and yrms of pointing 1 epoch for all detectors . . .	17
2	table xrms and yrms of pointing 1 and detector 2	18
3	Stellar populations (table taken from Cioni et al.2013)	19
4	counts of different populations in field LMC8_8	20
5	median proper motion of galaxies in all three fields	25
6	proper motion of population LMC 8.8. corrected for galaxy proper motion	29
7	proper motion LMC field 8_8	33
8	values for centre of mass proper motion calculation	37
9	counts of sources of fields STR 1_1 and STR 2_1	39
10	proper motion of population LMC 8.8. already corrected for galaxy proper motion	41
11	proper motion of population STR 2_1.	44

```

\end{table}

# Input: /home/thomasa/space/propermotion_lmc_8_8/original/galaxies/pointing_1/detector_2/pointing_1_detector_2_epoch_0_galaxies.tab Reference:
/home/thomasa/space/propermotion_lmc_8_8/original/galaxies/pointing_1/detector_2/pointing_1_detector_2_epoch_7_galaxies.tab Number of tie points: 0
# Initial linear transformation
#   xref[tie] =      0. +      1. * x[tie] +      0. * y[tie]
#   yref[tie] =      0. +      0. * x[tie] +      1. * y[tie]
# dx: 0.00 dy: 0.00 xmag: 1.000 ymag: 1.000 xrot: 0.0 yrot: 0.0
#
# Matched triangles transformation
#   xref[tie] = -14.94327 +      1.00008 * x[tie] + -8.5544E-5 * y[tie]
#   yref[tie] =  21.46286 + 6.03738E-5 * x[tie] + 0.9999465 * y[tie]
# dx: -14.94 dy: 21.46 xmag: 1.000 ymag: 1.000 xrot: 0.0 yrot: 0.0
#
# Column definitions
# Column 1: X reference coordinate
# Column 2: Y reference coordinate
# Column 3: X input coordinate
# Column 4: Y input coordinate
# Column 5: Reference line number
# Column 6: Input line number

596.1744385   81.8206863   611.2141724   60.3131714   349   428
1820.1866455  82.0465317   1834.7159424   60.5051727   142   169
946.7724609   82.4570999   961.7135010   60.9306259   242   292
1861.5212402  85.3347015   1876.4852295   74.0025024   339   417
450.4310608   98.1836014   465.1911316   76.7673035   364   446
1254.1470947  110.6016083  1269.2629395   88.9008026   16   21
446.6016541  112.0872421  461.6063843   90.7295074   29   37
900.6655884  112.3640289  915.8615112   90.9878769   377   463

```

```
# Fri 14:02:27 27-Jan-2017
begin/home/thomass/space/propermotion_lmc_8/IRAP/ref_epoch_0/matches/pointing_1/detector_8/pointing_1_detector_8_matching0-3.tab
xrefmean 1010.971065097003
yrefmean 1031.19434431417
xmean 1011.578052987739
ymean 1029.482400526976
geometry general
function polynomial
xshift 0.4369438475513968
yshift -1.902817172179391
xmag 1.000075237415172
ymag 0.9999944170242186
xrotation 359.9893246645728
yrotation 0.005002027096215226
xrms 0.2129591854498161
yrms 0.2047796694060928
surface1 11
3. 3.
2. 2.
2. 2.
0. 0.
0. 0.
2048. 2048.
0. 0.
2048. 2048.
0.4369438475513968 -1.902817172179391
1.000075237415172 1.863337701581798E-4
8.730135390159744E-5 0.9999944170242186
surface2 0
```